An-Najah National University

Faculty of Graduate Studies

Electronic, Structural and Magnetic Properties of $Al_{1-x}Mn_xN$ in Zincblende Structure:

First-Principle Study

Prepared by

Raed Tawfeeq Aref Jaradat

Supervised by

Dr. Mohammed Salameh Salem Abu-Jafar

Dr. Abdel-Rahman Mustafa Abu-Labdeh

This Thesis is Submitted in Partial Fulfillment of the Requirements for the Degree of Master of Science in Physics, Faculty of Graduated Studies, An-Najah National University, Nablus, Palestine.

2009

Electronic, Structural and Magnetic Properties of $Al_{1-x}Mn_xN$ in Zincblende Structure:

First-Principle Study

by

Raed Tawfeeq Aref Jaradat

This thesis was defended successfully on 24/06/ 2009 and approved by

Committee Members	Signature
1- Dr. Mohammed S. Abu-Jafar (Supervisor)	.....
2- Dr. Abdel-Rahman Abu-Labdeh (Co-Supervisor)	.....
3- Dr.Khawla-Qamhieh (External Examiner)	.....
4- Dr. Musa El-Hasan (Internal Examiner)	.....

Dedication

To the Memory of my Mother.

To my father who was a constant inspiration to me.

To my wife who always encourages me to further my study.

To my brothers and sisters.

To my children: Qusay, Shaimae, Boraq, Ameen and Qasem.

In the very beginning I'd like to express my gratitude to my supervisors Dr. Mohammed S. Abu-Jafar and Dr. Abdel-Rahman Abu-Labdeh for their valuable guidance and supervition. Also I am grateful to Dr. Musa El-Hasan for his guidance.

I'd like to thank all my Teachers at An-Najah National University, and special thanks to my group at my faculty. My thanks go as well to the members of the jury.

اقرار

أنا الموقع ادناه مقدم الرسالة التي تحمل العنوان:

Electronic, Structural and Magnetic Properties of $Al_{1-x}Mn_xN$ in Zincblende Structure: First-Principle Study

اقر بان ما اشتملت عليه هذه الرسالة انما هي نتاج جهدي الخاص، باستثناء ما تمت الاشارة اليه حيثما ورد، وان هذة الرسالة ككل، او اي جزء منها لم يقدم من قبل لنيل اية درجة او لقب علمي او بحث لدى اي مؤسسة تعليمية او بحثية اخرى .

Declaration

The work provided in this thesis, unless otherwise referenced, is the researcher's own work, and has not been submitted elsewhere for any other degree or qualification.

Student's name: اسم الطالب:

Signature: التوقيع:

Date: التاريخ:

Contents

List of Table

List of Figures

Electronic, Structural and Magnetic Properties of $Al_{1-x}Mn_xN$ in Zincblende Structure: First-Principle Study

By

Raed Tawfeeq Aref Jaradat

Supervisor

Dr. Mohammed S. Abu-Jafar **Dr. Abdel-Rahman M.Abu-Labdeh**

Abstract

We apply a First-Principles method to calculate the electronic structure and magnetic properties of the semiconductors $Al_{1-x}Mn_xN$ alloys by taking the concentrations (0.0, 0.25, 0.50, 0.75 , 1.00) in the zincblende structure (ZB), using a self-consistent full-potential linearized augmented plane-wave (FP-LAPW) method within the local-spin-density functional approximation (LSDA) and the generalized gradient approximation (GGA). Local spin density approximation (LSDA) and the generalized gradient approximation (GGA) are used to treat the exchange correlation energy.

We studied the evolution of the band structure and magnetic moment as a function of the lattice parameter of the MnN compounds and the ternary alloys $Al_{1-x}Mn_xN$. The binary compound MnN and also the ternary alloys with(x=0.5 and 0.75) magnetization increases as the lattice parameter increase and tend to saturate at the value $4\mu_B$ for MnN and 8 μ_B for the ternary alloys, as the material lattice (MnN) expansion the material goes from paramagnetic to ferromagnetic phase. We also found that the ternary alloy with x=0.25 is ferromagnetic and candidate to be half-metallic material, the majority spin states are metallic and the minority spin stats are insulating, for the other concentrations(x=0.5 and 0.75)

these are found to be ferromagnetic semimetals, the bands are crossing the Fermi energy for both spin up and spin down (majority spin and minority spin) (the Fermi level lies in the band).

The total energy versus lattice constant is obtained using the spin density functional theory. It was found that the equilibrium lattice parameter and the total magnetic moment strongly depend on concentration of Manganese atoms.

Chapter one

Introduction

A semiconductor is a material that has electrical conductivity in between that of a conductor and that of an insulator. Semiconductors are tremendously important in electronic technology. Semiconductor devices (electronic components made of semiconductor materials) are essential in modern consumer electronics, including computers, mobile phones, and digital audio players. Silicon is used to produce most semiconductors commercially, but dozens of other materials are used as well. Magnetic semiconductors are materials that exhibit both ferromagnetism (or a similar response) and useful semiconductor properties. Spin Magnetic moment is due to the spin of an electron around its own axis. This spin generates a magnetic dipole moment known as the Bohr magneton μ_B [**1**]. μ_B is given by the formula $\mu_B = \frac{e\mathbf{h}}{2m}$, where μ_B = 9.27 10^{-24} J/Tesla, e is the electronic charge, m is the electronic mass, and ħ is the reduced Planck's constant (ħ = 1.05×10^{-34} J/s).

Semionductors can be classified into three categories:

Conventional semiconductors, magnetic semiconductors and dilute magnetic semiconductors. Conventional semiconductor compounds such as elements from group IV of the periodic table, III-V and II-VI compounds. Magnetic Semiconductors (MSs) are conventional semiconductor compounds which doped with high concentration of magnetic ions, so these compounds have both ferromagnetic and semiconducting properties, due to a periodic array of magnetic ions in their crystal structures. In an effort to combine the benefits of the magnetic, electronic, and optoelectronic areas, a new class of material has recently been

demonstrated. Dilute magnetic semiconductors (DMSs), conventional semiconductor compounds which doped with low concentration of magnetic ions, are projected to be the basis for devices that rely on the manipulation of both the charge and spin of electrons moving in a semiconductor host. The main focus of the DMSs area is to effectively incorporate magnetic ions into a semiconductor lattice and produce a ferromagnetic material.

In DMSs and MSs the host semiconductor is doped with magnetic impurities, generally atoms of a transition metal such as manganese, iron, cobalt, or chromium. The main attraction of DMSs and MSs is the potential for incorporation into presently used semiconductor-based devices**.** Due to their half-metallicity and structural similarity to semiconductors, they are hopeful materials for a future spin-polarized electronics (spintronics); Spintronics is a field which uses the spin of carriers in addition to the charge of carriers to achieve new functionalities in electronic devices. In terms of spin injection efficiency, DMSs would provide an advantage over ferromagnetic metals in semiconductor devices [2, 3]. III-V compounds are compounds with two elements one from the III group in the periodic table and another from V group.

Mn doped in III-V compounds, as AlN and GaAs, are among the most widely studied. The electronic structure and mechanism of ferromagnetic in DMSs or MSs systems such as AlMnN are far from being completely understood. The attractive and principal idea is the manipulation of the spin of the electron, in addition to its charge, as an added degree of freedom [4, 5, 6, 7]. So far, most of the works have focused on GaMnAs or InMnAs DMSs [8]. As a result, the number of

possible new electronic devices and materials for more application and the quality of the existing devices is increasing much more.

The elements Boron (B), Aluminum (Al), Gallium (Ga) and Indium (In) are forming compound with Nitrogen (N) having the composition III-N semiconductors. The chemical bond of these compounds is predominant covalent, that is, the constituents develop four tetrahedral bonds for each atom. In recent years, group III-N have attracted the interest of many researchers due to their scientific and technological applications. III-N compounds, as AlN and InN, are very important to be studied because they have d-electrons which play in hybridization, covalent bonds and has a band gap ranges from 0.7 eV for InN to about 6.2 eV for AlN [1]. This means that there is a high probability for electrons to make transition from the valence band to the conduction band. There is considerable current interest in these materials because they appear to have great potential for use in spintronics. When magnetic semiconductors are implemented in devices, they could provide a new type of control of conduction. Whereas traditional electronics are based on control of charge carriers (n or p type). Practical magnetic semiconductors would also allow control of quantum spin state (up or down), which is an important property for spintronics applications. The availability of materials exhibiting ferromagnetism above room temperature is prerequisite for realizing such devices [1, 6, 7].

The possibility of the use of both charge and spin of the electron suggests many unprecedented functionality semiconductor devises such as spin qubits[9] (which can be used as the basic building block for quantum computing), spin valves[10] (which would result in high-density non-volatile semiconductor memory chips), spin field effect transistors

[11] (which could allow for software reprogramming of the microprocessor hardware during run time), and new generation magnetic random access memories (MRAM)[11]. The aim nowadays in experimental and theoretical research in this area is to identify materials that can be high-efficiency sources of charge carriers with well defined spin [12], and to produce (a class of) all semiconductor spin- dependent devices.

Group III-Nitrides (binaries InN, GaN, AlN and their alloys) are considered as the promising semiconductor material system for short wavelength light emitters and laser diodes. Their applications ranging from blue, green, and white light emitting diodes (LEDs) to blue laser diodes (LD) has surfaced in the last decade. AlN and GaN based LEDs are deemed as the next generation solid state lighting technology which will revolutionize architectural lighting. In addition to optoelectronic applications, high power and high frequency field effect transistors have also been developed utilizing this material system. Large band gap III-N materials, as AlN and InN, gives them distinct capabilities for use in high-power electronic and optoelectronic applications. Many device technologies, however, will require band-gaps larger than that of GaN. Large band-gap of AlN makes it an attractive material for investigation. Current applications of AlN include metal-insulator semiconductor, gas sensors, heterojunction diodes, optical detectors, and ultraviolet (UV) LEDs and lasers.

AlN is a ceramic and refractory material and has a combination of attractive physical properties, such as high melting point (3487K$^{\circ}$), high thermal conductivity, insulating properties (typical resistivity is around 10Ω.cm), large bulk modulus (high hardness), chemical and thermal

stability, and low thermal expansion. These properties beside its wide band gap lead to use this material in several electronic and optoelectronic applications (e.g., high-power field effect transistors) [13, 14, 15].

Several differences between III-N and the other III-V compounds make them have these physical and electrical properties, which can be related to the Nitrogen atom properties. The small covalent radius of the N atom (0.7A°) compared with the group V atoms (1.1 A°, 1.18 A°, 1.36 A° for P, As, and Sb, respectively) gives rise to the formation of short bond (4.37A° for AlN), with a large band energies (2.28eV for AlN). This leads to high melting temperature for AlN [16, 17, 18].

The group III-N AlN, GaN and InN can be crystallizing in the three phase's wurtzite (WZ), zincblende (ZB) and rocksalt (RS). At ambient conditions, the thermodynamically stable phase is the wurtzit structure. A phase transition to the rock salt structure takes place at high pressure. In contrast, the zinc-blend structure is metastable and may be stabilized only by heteroepitaxid growth on substrates reflecting topological compatibility. Although the ZB phase is not the ground-state structure for these materials [18, 19, 20, 21], researchers find interesting to study them in the ZB structure, since in it the Mn atoms find the same local environment as in diluted alloys, such as GaMnAS, GaMnN, or AlMnN [20]. Therefore, they studied the binary compounds AlN and MnN in the ZB structure in order to have a better understanding of the nature of AlMnN. The growth of AlN having excellent crystalline quality, smooth surface morphology and good electrical and optical properties as required for device fabrication however stills a big challenge. In recent years, variation growth techniques have been reported by several groups [22, 23, 24].

Thapa *et al* [13] studied the relation between basic epitaxial parameters. They reported the effects of the variation of basic growth parameters in low-pressure metalogranic vapor phase epitaxy (LP-MOVPE) on the surface morphology and crystal quality. At the early stage, hexagonal pits of varying size, depth and diameter, are largely observed and it was inferior layers. By optimizing growth parameters they were succeeding in reducing the pits concentration from $4x10^{10}$ Cm^{-2} to $3x10^{7}$ Cm^{-2}. On other hand there is worldwide interest in producing high-quality crystals suitable for nitride based electronic and optoelectronic devices. The ideal substrate should be lattice matched, isomorphic, and thermal expansion coefficient matched to the film as much as possible. Single crystal AlN is attractive as a substrate for group III-Nitride epitaxial growth due to its relatively small lattice, good thermal stability (melting point >2500 °C), high resistivity and similar coefficient of thermal expansion [25].

Manganese Nitride (MnN) was studied by Pavia *et al* [23, 26]. They studied the density of states and the magnetic moments as a function of the lattice parameter. They found that MnN is a half- metallic (i.e., showed a band gap at the Fermi energy for one spin direction when the lattice expanded). Indeed, they found that the magnetic moment of MnN vary with lattice constant. It begins from about zero at the equilibrium lattice parameter to $4.0\mu_B$ at large lattice parameter. Also they concluded that the equilibrium lattice parameter with Generalized Gradient Approximation GGA is greater than with local spin density approximation LSDA.

DMSs and MSs related to Mn-doped III-V compound semiconductors have attracted much attention because of the combining

of magnetic and semiconducting properties, and hence due to their potential application in developing future spintronic devices [27, 28]. Recently DMSs based on III-V compound have been extensively studied because of the success in doping high concentration of transition metal ions by molecular beam epitaxy (MBE) [29]. Most remarkably, Mn doping in InAS, AlN, GaN and GaAs lead to ferromagnetism [30]. This behavior is generally called carrier-induced ferromagnetism because holes carriers introduced into the system mediate the ferromagnetic coupling between the Mn ions [31], although its microscopic mechanism has been controversial. The key to understand the mechanism of the carrier-induced ferromagnetism is to elucidate the nature of the doped hole carrier as well as the exchange interaction between the host valence band and the localized d-orbitals of the magnetic ions. Injection of spin-polarized holes has been observed experimentally [32, 8] and supported theoretically [33, 34], proving that spintronic devices are feasible. However a problem of these DMSs-systems is that the Curie temperatures are well below room temperature (e.g., 170 K$^{\circ}$ for Ga MnAs). This is the major obstacle for applications [1, 35]. Recently, a Curie temperature of more than 340 K$^{\circ}$ has been observed for AlCrN [36, 37] and greater than 300 K$^{\circ}$ for AlMnN [38].

The fabrication of ferromagnetic AlN would produce a wider range of possible all semiconductor spin-dependent devices, for example ferromagnetic AlMnN could be used as a magnetic barrier in a tunnel junction, where it would serve as spin filter. When AlN or GaN is alloyed with a transition metal element such as Mn, the Al, Ga cation is substituted by the Mn atom. When Mn atoms form a homogeneous solid solution in AlN the resulting structure becomes ferromagnetic depending

on the Mn concentration [39]. The observed ferromagnetism is attributed to the coupling of the spins of the carriers in the system with the localized spins of the Mn ions resulting in a long range order. In other words, the delocalized conduction band electrons and/or valence band holes interact with the localized magnetic moments associated with the localized magnetic moments of the Mn ions. In more scientific terms this is called the s-d exchange interaction for the case of conduction band electrons and the localized 3d states of the Mn ions, and p-d exchange interaction for the valence holes and the localized 3d states of the Mn ions. On the other hand, the coupling between Mn ions is antiferromagnetic and counteracts the previous mechanism [39].

Frazier *et al* [40] reported room temperature ferromagnetism in single phase AlMnN grown by gas-source molecular beam epitaxy. The lattice constant was found to decrease with the Mn content, suggesting that the Mn occupies a substitutional site. It was estimated that the AlMnN films contained no more than 1% Mn. This single phase AlMnN was found to be p-type, in accordance with what is expected for a deep-acceptor produced by substitutional Mn. This expected deep-acceptor nature of Mn in AlN was taken as a suggestion that carrier-mediated ferromagnetism would be unlikely. The presence of Mn4N compound , that could clustering in AlMnN, was discarded the analyses of the magnetizations as a function of temperature for AlN, single phase AlMnN, and Mn4N (grown under the same conditions as the previous materials) show substantially different behaviors. In fact Mn4N clearly has a ferromagnetic behavior, and the formation of clusters has been proposed as the case of hysteresis in some ferromagnetic III-V materials [26, 41]. Therefore, the incorporation of Mn into the AlN lattice forming the ternary AlMnN was concluded to be the most likely reason for the

observed hysteresis. In another work, Frazier *et al* [42] reported the properties of Mn implanted AlN (0.03 Mn) and estimated a saturation magnetic moment of $0.17\mu_B$. Disorder effects induced by the implantation process were supposed to contribute in producing a distribution of exchange coupling that favors antiferromagnetism, and reduce the effective magnetism of the sample. It was also argued that the origin of the observed ferromagnetism is not likely to be carrier mediated, due to the insulating nature of AlN. On the other hand, ferromagnetism could occur due to a midgap defect band [43]. Another possibility for the observed magnetic properties could be the presence of atomic scale clustering of Mn atoms resulting in localization of spin-polarized holes near region of higher Mn concentration [43, 44].

Pavia *et al* [45] studied the electronic structure and magnetic properties of $Al_{1-x}Mn_xN$ dilute magnetic alloys in the ZB structure with x = 0.063 and 0.031. They applied a first principles method based on the density functional theory within the local spin density approximation, and the full potential linear augmented plan-wave method to calculate the electronic structure and magnetic properties of $Al_{1-x}Mn_xN$ dilute magnetic alloys in the ZB phase. They concluded that Mn in the dilute doping limit form near mid-gap deep levels in the ZB AlN. They noted that ferromagnetic ZB phase $Al_{1-x}Mn_xN$ alloys are candidates to be half-metallic materials, (the majority spin states are metallic and the minority spin states are insulating). They also included that the total magnetization of the cell is $4.0\mu_B$ and it dose not vary with concentration.

Kanoun *et al* [46] studied the electronic structure and magnetic properties of $Al_{1-x}Mn_xN$ (x= 0, 0.25) in ZB structure using Full Potential Linearized Augmented Plane Wave plus Local Orbitals (FP-LAPW+lo).

They found that the majority spin states are metallic but the minority spin states are insulating. Also the total magnetization of the cell was evaluated as $4.0\mu_B$ per unit cell for x=0.25 and zero for x=0.0. As a result they concluded that the valence band is ferromagnetically coupled to the Mn atoms, so with x=0.25 this alloy is a half-metallic ferromagnetism alloy but it is insulator with x=0.0.

In order to help understanding and give a detailed description of the electronic and magnetic properties of $Al_{1-x}Mn_xN$ compounds (x=0, 0.25, 0.5, 0.75 and 1), we use in the present work one of the most accurate methods (which is Full-potential linearized augmented plane wave (FP-LAPW)[47, 48] approach based on the density functional theory [49] within the local spin density approximation (LSDA) and the Generalized Gradient Approximation (GGA) using scheme of Perdew, Brouke and Ernzerhof [50])to study the ground states properties of $Al_{1-X}Mn_XN$ and compare between GGA and LSDA calculations. As mentioned before, to our best knowledge no one study these alloys with concentrations x>0.25.

The layout of this thesis is as follows.

Chapter two present the basics of Density Functional Theory DFT and FP-LAPW+lo. Computational details used in this work are presents in chapter three. In chapter four we report and discuss our results obtained for the $Al_{1-x}Mn_xN$ (x=0, 0.25, 0.5, 0.75, 1.0). The results and conclusions are summarized in chapter five.

Chapter two
Density functional theory

2.1 Introduction

In solids, one often starts with an ideal crystal that is studying (relative stability, chemical bonding, relaxation of atoms, electrical, phase transition, optical or magnetic behavior) on atomic scale at zero temperature. The unit cell may contain several atoms at certain positions and is repeating with periodic boundary conditions.

So the theorists came to face a many-body problem, and because these particles are so light compared with classical scale, it is a quantum many body problem. In principle, to study the materials and their properties the theorist has to solve the time independent Schrödinger equation.

$$\hat{H}\, y \;=\; E\, y \tag{2.1}$$

Hear, ψ is the wave function of all participating particles and $\hat{H}$ is the many-particles Hamiltonian for this system. $\hat{H}$ Can be written as

$$\widehat{H} = -\frac{\hbar^2}{2}\sum_i \frac{\nabla^2_{\overrightarrow{R_i}}}{M_i} - \frac{\hbar^2}{2}\sum_i \frac{\nabla^2_{\overrightarrow{r_i}}}{m_e} - \frac{1}{4\pi\epsilon_0}\sum_{i,j}\frac{e^2 Z_i}{\mid \overrightarrow{R_i} - \overrightarrow{r_j} \mid} + \frac{1}{8\pi\epsilon_0}\sum_{i\neq j}\frac{e^2}{\mid \overrightarrow{r_i} - \overrightarrow{r_j} \mid} + \frac{1}{8\pi\epsilon_0}\sum_{i\neq j}\frac{e^2 Z_i Z_j}{\mid \overrightarrow{R_i} - \overrightarrow{R_j} \mid} \tag{2.2}$$

The mass of the ion at R_i is M_i, the mass of the electron at r_i is m_e. The first term in equation (2.2), is the kinetic energy operator for the nuclei (T_n), the second for electrons (T_e), the last three terms correspond to coulomb electron-nuclear attraction (V_{en}), electron-electron repulsion (V_{ee}) and nuclear-nuclear repulsion (V_{nn}), respectively.

There is not an exact solution to this Schrödinger equation. The problem of this many body particle is the dependence of its wave function on the coordinates of each particle. We solve the problem using some approximations.

These approximations are:

2.2.1 The Born-Oppenheimer approximation

Born-Oppenheimer approximation is one of the most important approximations. The approximation began with the idea that the nuclei are much massive in comparison to the electrons and so that much slower than the electrons, this means that the kinetic energy of the nuclei is much smaller and approximately goes to zero. In other words they consider being static, only the electrons are kept as players in this many body problems [51]. The nuclei are reduced to a given source of positive charges; they become ‘external’ to the electron cloud. So in equation (2.2) we can neglect the first term and the last term reduces to constant.

After the application of this approximation the problem is left with a collection of interacting negative particles, moving in the potential of the nuclei. Therefore the many body problems are left with the kinetic energy of the electron gas (T_e), the potential energy due to electron-

electron interactions (V_{ee}) and the potential energy of the electrons in the (now external) potential of the nuclei (V_{ext}). So the new many body Hamiltonian can be formally written as:

$$\hat{H} = \hat{T}_e + \hat{V}_{ee} + \hat{V}_{ext} \qquad (2.3)$$

The many body problem obtained after Born-Oppenheimer approximation is much simpler than the original one, but still difficult to solve. It needs more simplifications.

2.2.2 Hartree and Hartree-Fock Approximation

In Hartree approximation **[52]**, the solution of many-electron problem can be solved by assuming the electrons are independent from each other. By this assumption the total wave function for the electrons can be written as:

$$\Psi(r_1,r_2,r_3\ldots.r_N) = \Psi_1(r_1)\Psi_2(r_2)\Psi_3(r_3)\ldots. \Psi_N(r_N) \qquad (2.4)$$

where $\Psi_N(r_N)$ is the electron wave function. With this assumption the electron density can be represented by.

$$r(r) = \sum_{i=1}^{N} \left| y_i(r) \right|^2 \qquad (2.5)$$

After this assumption the total Hamiltonian can be written as:

$$(T_s + V_{ext} + V_H)\Psi(r) = E\Psi(r) \qquad (2.6)$$

where T_s is the single particle kinetic energy, V_H is the Harttree potential, (the component of the electron-electron potential), and is given by.

$$V_H = \frac{1}{8pe_0} \sum_{ij} \frac{\left|y(r_i)\right|^2 \left|y(r_j)\right|^2 d^3 r_i d^3 r_j}{\left|\mathbf{r}_i - \mathbf{r}_j\right|} \qquad (2.7)$$

Hartree assumption is the electrons are non-interacting; so there exists a non-zero probability of finding two electrons occupying the same point in space.

Later this wave function is modified to include the spin of the electron by the Hartree-Fock approximation **[53]**. This approximation is an extension of the above Hartree approximation to include the permutation symmetry of the wave function which leads to the exchange interaction. Exchange is due to the Pauli Exclusion Principle, which states that the total wave function for the system must be antisymmetric under particle exchange. Therefore no two electrons can have the same set of quantum numbers, and electrons with the same spin cannot occupy the same state simultaneously.

2.2.3 Density Functional Theory

The well-established scheme to calculate electronic properties of solids are based on the density functional theory (DFT), for which formally established in 1964 by two theorems due to Hohenbery and Walter Kohn **[54]**. DFT is a universal approach to quantum mechanical many-body problem, where the system of interacting electrons is mapping in a unique manner onto an effective non-interacting system that has the same total density. The great success of the density functional theory for the description of the ground-state properties of large material classes including insulators, semiconductors, semimetals, half-metals (half-metals are defined as magnetic materials showing a band gap at the Fermi energy

for one spin direction), simple metals, transition-metals and rare-earths metals. The ground state electron density ρ(r) defines the total energy E, must be a function of the density.

$$E = E(\rho) \qquad (2.8)$$

The density contains as much information as the wave function does, (relative stability, chemical bonding, relaxation of atoms, electrical, phase transition, optical or magnetic behavior) could possibly known. All observable quantities can be constructed in a unique way from the density only, therefore they can be written as function of the density.

Hohenberg and Kohn showed that the true ground state density is the density that minimizes E (ρ) and the other ground state properties are also functional of the ground state density. In addition, theorists can do on spin-polarized system where E and the other ground state properties become functional of both spin up and spin down densities.

$$E = E(\rho_{\downarrow}, \rho_{\uparrow}) \qquad (2.9)$$

The non-interacting particles of this system move in an effective local one-particle potential. This potential consists of a classical mean-field (Hartree) part and a quantum mechanical part which is an exchange-correlation part V_{xc} , that incorporates all correlation effects exactly. So E (ρ) is rewritten as the Hartree total energy plus another smaller unknown functional called exchanged-correlation functional, E_{xc} (ρ).

$$E(\rho) = T_s(\rho) + E_c(\rho) + E_H(\rho) + E_{ii}(\rho) + E_{xc}(\rho) \qquad (2.10)$$

where T_s (ρ) represents the single particle (non interacting) kinetic energy, E_c (ρ) denotes the Coulomb interaction energy between the electrons and the nuclei, E_{ii} (ρ) term represent from the interaction of the nuclei with each other and E_H (ρ) is the Hartree component of the electron-electron energy.

$$E_H(r) = \frac{e^2}{2}\int d^3r d^3r' \frac{r(\mathbf{r})\, r(\mathbf{r}')}{|\mathbf{r}-\mathbf{r}'|} \qquad (2.11)$$

and E_{xc}(ρ) is the exchanged-correlation energy given by

$$E_{XC}(\rho(r)) = \int \rho(r)\, \varepsilon_{XC}\, d\rho(r) \qquad (2.12)$$

where ε_{XC} (ρ(r)) is the exchange-correlation energy per particle of the homogeneous electron gas.

According to the variational principle, a set of effective one-particle Schrödinger equation, (the so-called Kohn-Sham (KS) equations [**55**]) must be solved. Its form is

$$[T_s + V_{ext}(r) + V_H(\rho(r)) + V_{XC}(\rho(r))]\Phi_i(r) = \varepsilon_i \Phi_i(r) \qquad (2.13)$$

where, ε_i is the single particle energy and $\Phi_i$is the electron wave function.When written in Rydberg atomic units for an atom with the obvious generalization to molecules and solids. The four termes represent the kinetic energy operator; V_H is the Hartree potential, V_{ext} the coulomb potential and V_{XC} is the exchange-correlation potential.

V_H can be written as:

$$V_H = \int \frac{r(r')}{|\mathbf{r}-\mathbf{r}'|} dr'$$

(2.14)

Again we can write the Schrödinger like equations in a new form

$$(-\frac{\mathbf{h}^2}{2m}\nabla^2 + V_{eff}(\mathbf{r}))\Psi(\mathbf{r}) = E\Psi(\mathbf{r}) \qquad (2.15)$$

where Ψ (r) is the total wave function of all electrons, E is the total energy and V_{eff} is the effective potential and given in equation (2.16).
Equation (2.14) transforms the many-particle problem into a problem of one electron moving in an effective potential such that

$$V_{eff}(\mathbf{r}) = V_{ext}(\mathbf{r}) + \int \frac{r(r')}{|\mathbf{r}-\mathbf{r}'|} dr' + \frac{dE_{xc}(r)}{dr} \qquad (2.16)$$

where the second term represents the Hartree potential V_H given in equation (2.14) and the third one represent the exchange-correlation potential V_{XC}.

The KS equations must be solved iteratively until self-consistency is reached. The iteration cycles are needed because of the interdependence between orbitals and potential.

From the electron density equation (2.5) the V_{ext} and V_{XC} potentials for the next iteration can be calculated, which define the KS orbitals. This closes the self-consistent loop. The exact functional form of the potential V_{XC} is not known and thus one needs to make approximation. Local (spin) density approximation (L(S)DA) approximation solve this problem and it perform well with systems those varying density slowly . A logical step to

improve on L(S)DA by making the exchange-correlation potential depending on the local density of local volume as in L(S)DA and also on the density of the neighboring volume by adding gradient term of the electron density. This modern version of DFT called Generalized Gradient Approximation (GGA), and it reach to a high accuracy.

2.3 Single particle Kohn-Sham equation

Nearly all approaches that have been proposed for solid, including Linearized augmented plane wave method LAPW which will discuss in the next chapter do rely on a basis set expansion for the KS orbitals. With Hartree-Fock HF or DFT one ends with an infinite set of one electron equations of the form of equation (2.13).

The similarity between the HF and KS equations means that the same mathematical techniques can be used to solve them. Solving the equation means we want to find the coefficients C_{in} to express φ_n in a given basis set . $f_i(\mathbf{r})$

$$j_n(r) = \sum_i C_{in} f_i(r) \qquad (2.17)$$

Hear φ_n are mathematical true of one electron (or single particle) orbitals. The solution of the KS orbitals permits to determine the C_{in} for the occupied orbitals that minimize the total energy. In practice one works with a limited set of basis functions. Such a limited basis will never be able to describe φ_n exactly, but one could try to find a basis that can generate a function that is 'close' to φ_n.

Density functional calculation required the optimization of the C_{in} and the determination of the density Figure 2.1. This procedure is usually performed separately and hierarchically. Using stander matrix techniques

it is possible to repeatedly determine the C_{in} that solve the single equation (2.17) for affixed charge density. Hence, given the basis, the Hamiltonian and the overlapping matrix, H and S, can be constructed and the following matrix eigenvalue equation

$$(H - \varepsilon_i S)C_{in} = 0 \qquad (2.18)$$

or in another form

$$\begin{pmatrix} \langle j_1|H|j_1\rangle - e\langle j_1|j_1\rangle & \mathbf{K} & \mathbf{L} \\ \mathbf{M} & \langle j_i|H|j_j\rangle - e\langle j_i|j_j\rangle & \mathbf{M} \\ \mathbf{M} & \mathbf{M} \quad \mathbf{M} & \mathbf{M} \\ \mathbf{L} & \mathbf{L} & \langle j_i|H|j_i\rangle - e\langle j_i|j_i\rangle \end{pmatrix} \begin{pmatrix} C_1^n \\ \mathbf{M} \\ C_i^n \end{pmatrix} = \begin{pmatrix} 0 \\ \mathbf{M} \\ 0 \end{pmatrix} \qquad (2.19)$$

The overlap matrix S, defined as

$$S^{n,n'} = \int_{\Omega} j_n^*(\mathbf{r}) j_{n'}(\mathbf{r}) d^3r = \langle j_n | j_{n'} \rangle \qquad (2.20)$$

So it is diagonal and it is equal $S=\delta_{n,n/}$; hear Ω is the volume of the unit cell . Equation (2.19) is solved for each K-point in the irreducible wedge of the Brillouin Zone. The optimized C_{in} will yield the exact self-consistent solution only if the true occupied KS orbitals can be expressed as a linear combination of the basis functions. In the case where they cannot be expressed exactly in term of the basis, an approximate optimal solution will be found (the one that gives the lowest possible total energy for basis). Therefore, the quality of basis set can be measured by comparing how much the total energy evaluated with the orbitals of equation (2.18) differ from the true KS energy. The larger i, the better the approximation of the eigenfunction, but the more time-consuming the diagonalization of the matrix in equation (2.19), (2.20).

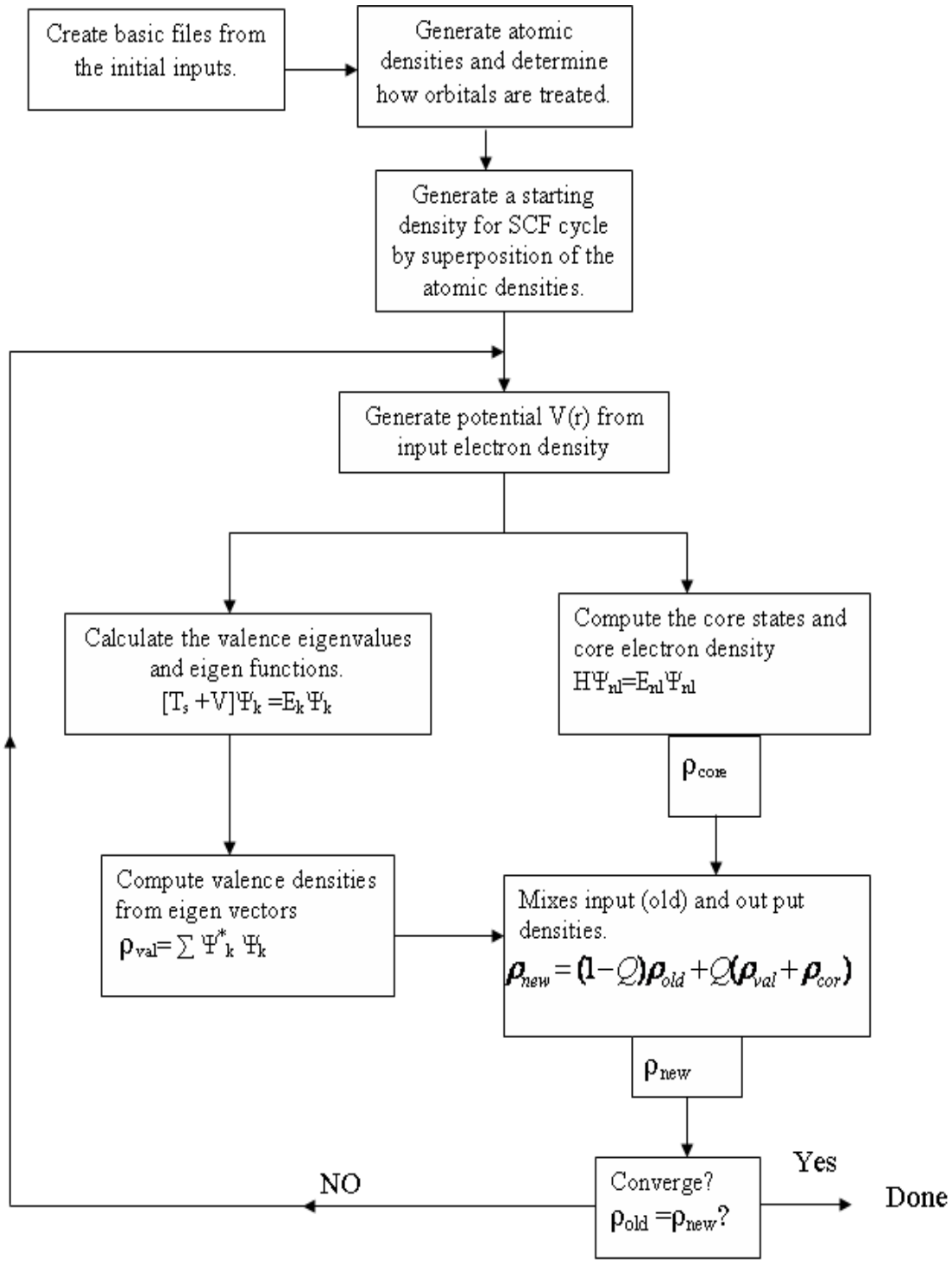

Figure 2.1: Flow chart for the self-consistent density functional theory.

2.4.1: The local spin density approximation LSDA:-

This approximation was applied to DFT by Kohn - Sham method [54].Local-spin density approximation (LSDA) (or simply local-density approximation (LDA)) dealing only with nonmagnetic systems) [56] is an

approximation used to calculate the unknown exchange-correlation energy EXC. This is the only term in the effective potential of the Kohn-Sham equation which is can't be determined exactly. It divides the inhomogeneous system into a small set of regions containing homogeneous interacting electron gas with density $r_s(\mathbf{r})$, where (σ) is the spin up↑ or spin down↓ ; and the total density ρ(r) =ρ↓(r) + ρ↑(r).

In each region the exchange-correlation energy per particle of the homogeneous gas can be stated as:

$$e_{XC}(r_\uparrow, r_\downarrow) \equiv e_X(r_\uparrow + r_\downarrow) + e_C(r_\uparrow + r_\downarrow) \qquad (2.21)$$

The analytic expression for the exchang energy εx(ρ↑,ρ↓)can be obtained from the Hartree-Foch approximation [57-59].The total exchange-correlation energy E_{xc}^{LDA} is the sum of the contribution of all regions [60], which is based on the quantum Monte-Carlo result of the ground-state energy for the homogenous electron gas [61]. The total exchange-correlation energy is the sum of the contribution of all regions:

$$E_{XC}^{LDA}(r_\uparrow, r_\downarrow) = \int r(\mathbf{r}) e_{XC}(r_\uparrow(\mathbf{r}), r_\downarrow(\mathbf{r})) d^3r \qquad (2.22)$$

The exchange-correlation potential is calculated from

$$V_{XC}^{LDA}(X) = \frac{dE_{XC}}{dr_s(\mathbf{r})} = e_{XC}(r_\uparrow, r_\downarrow) + \frac{de_{XC}(r_\uparrow, r_\downarrow)}{dr_s(\mathbf{r})}\left(r_\uparrow(\mathbf{r}) + r_\downarrow(\mathbf{r})\right) \qquad (2.23)$$

The derivative of $V_{XC}^{LDA}(X)$ expression is given by Painter [**62**].

2.4.2 Generalized gradient approximation

Many modern codes using DFT now use more advantage approximations to improve accuracy for certain physical properties. Generalized gradient approximation came as a modification of (LSDA); it inserts another parameter to the exchange-correlation energy E_{XC}; E_{XC} is a functional of local electron spin density ρ(r) and their gradients:

$$E_{XC}^{GGA}(r_{\uparrow}, r_{\downarrow}) = \int e_{XC}(r_{\uparrow}(\mathbf{r}), r_{\downarrow}(\mathbf{r}))r(\mathbf{r})\nabla r(\mathbf{r})dr^3 \qquad (2.24)$$

Because of the incorporating of local gradient a better description of system is expected [**63-65**]. The (GGA) improve significantly ground state properties of light atoms, molecules and solids and generally tends to produce larger equilibrium lattice parameters with respect to the LSDA.

2.5 Full potential Linearized Augmented Plane Wave plus Local Orbitals (FP-LAPW+LO).

2.5.1 Introduction

This section starts with an introduction of the Augmented Plane Wave method (APW) and Linearized augmented plane wave plus local orbitals method (LAPW+lo) concepts to solve the Kohn-Sham equation for a periodic solid. Then the concepts of full potential (FP) method and Muffin Tin approximation with full potential are described.

There are several techniques to solve the one-electron functions, the basis which are used in calculation are plane waves (PWs) that corresponding to Bloch functions. However, these plane waves need's augment because it inefficient basis set for describing the rapidly varying wave functions close to the nuclei.

2.5.2 The Augmented Plane Wave method (APW):-

Augmented plane wave introduced by Slater as a basis functions for solving one-electron equations. APW divide the unit cell into two regions, Figure 2.2:

i) non-overlapping spheres centered at the atomic sites.
ii) An interstitial region.
In the two types of regions different basis set are used.
Inside the atomic sphere i of radius R_i(close to the nuclei), the electrons behave quit as they were in a free atom, and radial function is used in the remaining interstitial region, in this region (far away from the nuclei) the electrons are free so plane waves are employed.

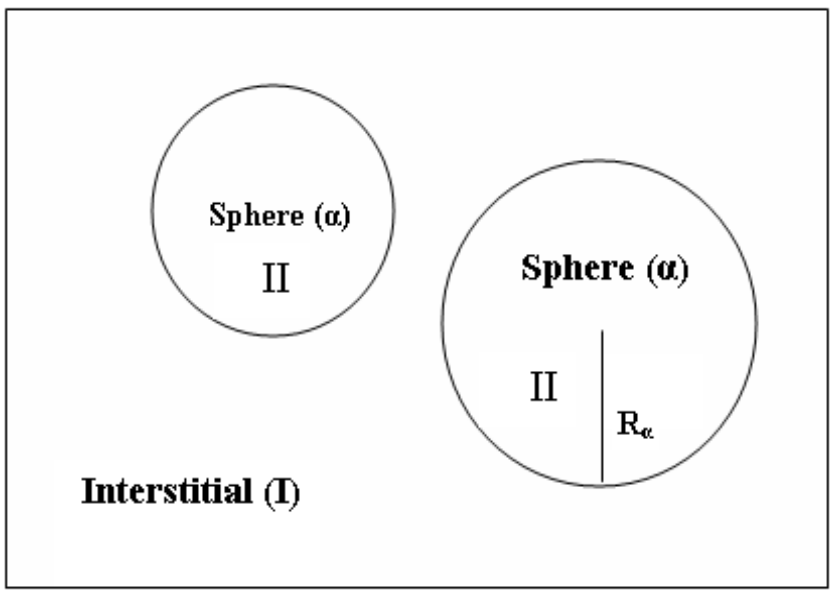

Figure 2.2: Adaptation of the basis set by dividing the unit cell into atomic spheres and interstitial regions.

These basis set is due to the fact that the potential and wave functions close to the nuclei are similar to those in an atom, while between the atoms they are smother. The APWs consist of:

$$f^{APW}_{K+G}\left(\mathbf{r}\right)=\begin{cases}\sum_{lm} A_{lm}\,u_{lm}(r,e)\,Y_{lm}(\mathbf{r}), & r \in \text{II}\\ \frac{1}{\sqrt{V}}\sum_{G} C_G \exp(\,i(\mathbf{k}+\mathbf{G}).\mathbf{r}), & r \in \text{I}\end{cases} \qquad (2.25)$$

where, is the wave function, V is the unit cell volume, is the position inside sphere with polar coordinates $f(\mathbf{r})$ $\mathbf{r}$, $\mathbf{k}$ is a wave vector in the first Brillouin Zone, $\mathbf{G}$ is the reciprocal lattice vector, $u_{lm}(r,\varepsilon)$ is the numerical solution to the radial Schrödinger equation at the energy ε and A_{lm}, C_G are expansion coefficients.

The KS orbitals $y_i(\mathbf{r})$ are expressed as a linear combination of APWs $f(\mathbf{r})$. Inside the MT sphere a KS orbital can only be accurately described if ε in the APW basis functions is equal to the eigen-energy ε_i. Therefore, a different energy dependent set of APW basis functions must

be found for each eigen-energy. C_G and A_{lm} are expantion coefficients; E_l is a parameter (set equal to the band energy) and V the spherical component of the potential in the sphere. The $u_{lm}(r)$ satisfy the following equation.

$$\left[-\frac{d^2}{dr^2}+\frac{l(l+1)}{r^2}+V(r)-E_l\right]ru_{lm}(r)=0 \qquad (2.26)$$

By these functions Slater noting that plane waves are the solution of the Schrödinger equation in a constant potential and radial functions are solution in a spherical potential. This approximation to the potential is called "muffin ten"(MT).

The dual representation defined by equation (2.25) is not guaranteed to be continuous on the sphere boundary, as it must be for the kinetic energy to be well defined. Accordingly, it is necessary to impose this constraint. In the APW method this is done by requiring that the augmented functions match (in value not in slope) the plane waves at the atomic sphere boundary.

This done in APW by defining the u_{lm} in term of C_G.

$$u_{lm}=\frac{4pi^l}{\sqrt{V}u_l(R)}\sum_G C_G J_l(|k+g|)Y_{lm}^*(\mathbf{K}+\mathbf{G}) \qquad (2.27)$$

where $J_l(|k+g|)$ is the Bessel function of order *l*.

The u_{lm} are determined by the plane wave coefficients (C_G) and the energy parameters E_l, which are variational coefficient, in APW method.

There is no restriction on the derivative at the atomic sphere boundary. Therefore, the APW basis functions have in general a kink at

$r=R_{MT}$ and their derivations are discontinuous at the boundary. One must mention hear that a more accurate method is the linearized augmented plane wave method (LAPW), which made the basis functions and their derivatives continuous by matching to a radial function at fixed E_l plus its derivative with respect to E_l.

A more accurate band structure calculation scheme is the Linearized Augmented Plane Wave (LAPW) method, which use the basis function and its derivatives.

2.5.3 Linearized augmented plane wave method (LAPW):-

A more flexible and accurate band structure calculation scheme is the LAPW method where the basis functions and their first derivatives are made continuous by matching to radial function at fixed E_l plus its derivative with respect to E_l, continuous at the boundary between core $r<R_a$ and interstitial region I. The linearized augmented plane wave method (LAPW) scheme introduced by Andersen **[66],** in this scheme a linear combination of radial function times spherical harmonics are used. The original energy dependence of the radial basis function is thereby replaced by the Taylor series:

$$u_l(r,e)=u_l(r,e_l)+(e-e_l)\frac{\partial u_l(r,e)}{\partial e}\Big|_{e=e_l}+o(e-e_l) \qquad (2.28)$$

The wave function $f(\vec{r})$ inside the sphere $r<R_a$ are linear combination of *u(r)* at affixed energy. Its energy derivative $\dot{u}(r)$ at the same energy E_l can be written as

$$f_{K+G}^{LAPW}\left(\mathbf{r}\right)=\begin{cases}\sum_{lm}[A_{lm}u_{lm}(r)+B_{lm}\dot{u}_{lm}(r)]Y_{lm}(\mathbf{r}), & \text{r} \in \text{ II} \\ \frac{1}{\sqrt{V}}\sum_{G}C_{G}\exp(i(\mathbf{k}+\mathbf{G}).\mathbf{r}), & \text{r} \in \text{I}\end{cases} \qquad (2.29)$$

where B_{lm} are coefficients for the energy derivative. The augmenting functions $u_{lm}(r)Y_{lm}(r)$ and their derivatives $\dot{u}_{lm}(r)Y_{lm}(r)$ are linearized to form the basis functions inside the spheres.In order to determine the coefficients A_{lm} and B_{lm}, we will require that the function in the sphere matches the plane wave both in value and in slope at the sphere boundary.

From the equation (2.29) it is obvious that a plane waves are used in the interstitial region of the unit cell I, in contrast a linear combination of radial functions times spherical Hamiltonian are used inside atomic sphere r<R. Two radial functions are used in LAPWs instead of one in the APWs, so LAPW are more variational freedom inside the atomic spheres, the basis functions and their derivatives must be continuous at the boundary. The u_l and its energy derivative satisfies the following equation

$$\left[-\frac{d^2}{dr^2}+\frac{l(l+1)}{r^2}+V(r)-E_l\right]r\dot{u}_{lm}(r)=ru_{lm}(r) \qquad (2.30)$$

The LAPWs are plan waves in the interstitial zone of the unit cell which match the numerical radial functions inside the spheres with the requirement that the basis functions and their derivatives are continuous at the boundary.

The linear compensation of $u_l(r)$ and its derivative are obtained by numerical integration of the radial Schrödinger equation on a radial mesh inside the sphere. There are two radial functions in LAPWs instead of one in APW, non-spherical potential inside spheres can now treated with no difficulties. On the other hand there is a price to be paid fore the additional radial function: the basis function must have continuous derivatives and consequently higher plan wave cut-offs are required to achieve a given level of convergence.

The solution of the KS equations is expanded in this combined basis according to the linear variation method:

$$y_k = \sum_n c_n j_{kn} \qquad (2.31)$$

The coefficients c_n are determined by the Rayleigh-Ritz variational principle. The convergence of this basis set is controlled by a cut-off parameter $R_{MT} \times K_{Max}$, where R_{MT} is the smallest atomic sphere radius in the unit cell and K_{Max} is the largest K_n vector in equation (2.31).

2.5.4 The augmented plane wave plus local orbitals method (APW+lo):

APW+lo (local orbital) method was proposed by Sjöstedt et al. **[67]**. The augmentation in this method is similar to it in APW scheme with a different that each radial wave function is computed at fixed linearization energy to avoid the non-linear eigenvalue problem that complicated the APW method, so only the condition of continuity is required. The local orbitals can be defined as

$$\phi(\vec{r}) = \begin{cases} \left[A_{lm}^{\alpha,lo} u_{lm}^{\alpha}(r) + B_{lm}^{\alpha,lo} \dot{u}(r) \right] Y_{lm}(\vec{r}), & r \in II \\ 0, & r \in I \end{cases} \qquad (2.32)$$

The two coefficients are determined by the normalization and the condition that the local orbital has zero value at the sphere boundary. There is no dependence between $\dot{u}_{lm}(r)$ and the PWs, since it is only included for a few local orbitals (e.g., p and d states) and not associated with every plan wave. This new scheme can reach the same accuracy as LAPW but converse faster in terms of number of PWs [68]. The highest efficiency was found for a mixed basis set in which the low *l*-quantum numbers are treated by APW+lo but the higher *l* by LAPW. Physical quantities such as the total energy, forces converge faster than with pure LAPW but reach the same values. If for each atom local orbitals for p and d-states are added, the basis set will slightly increase [69], this slightly increased computational time is a small price to be paid for the much better accuracy that local orbitals offer, and therefore they are always used [70].

2.5.5 The full potential calculation:

One of the most accurate schemes for solving the Kohn-Sham equations is the full-potential linearized augmented plan wave (FP-LAPW) method suggested by Andersen [71] on which WIEN cod is based. Full-potential LAPW method (FP-LAPW) combines the choice of the LAPW basis set with the treatment of the full-potential and charge density with out any shape approximations in the interstitial region and inside muffin-tins. This generalization is achieved be relaxing the constant interstitial potential V_I and the spherical muffin-tin approximation $V_{MT}(r)$ due to inclusion of a warped

interstitial $\sum V_I^K e^{ikr}$, where K are all reciprocal lattice victors up to the largest value of K_{Max}. The non-spherical terms inside the muffin-tin spheres:

$$V(\vec{r}) = \begin{cases} \sum_K V \quad e^{i\vec{k}\vec{r}} & \text{, Interstitial-region} \\ \sum_{lm} V_{lm}(r) Y_{lm}(\vec{r}) & \text{, muffin-tin} \end{cases} \tag{2.33}$$

This method become possible with the development of a technique for obtaining the coulomb potential for a general periodic charge density with out shape-approximation and with the inclusion of the Hamiltonian matrix elements due to the warped interstitial and non-spherical terms of the potential.

2.6.1 WIEN2K code

The program package WIEN2K allow performing electronic and magnetic structure calculations of solid by using density functional theory (DFT).its based on LAPW+lo method, among one of the most accurate schemes for band structure calculations. In DFT the local spin density approximation (LDA) or the improved version of the generalized approximation (GGA) can be used.

In the new version WIEN2K [48] (APW +lo) is used inside the atomic spheres for the chemically important orbitals, whereas LAPW is used for the others.

2.6.2: Self-Consistent Cycle (SCF)

The WIEN2k package Figure 2.1 consists of several independent programs, initialization and self-consistent cycle programs.The initialization programs used to determines the space group of the structure, generates free atomic densities, how the different orbitals are treated in the band structure calculations, generates a k-mesh in the irreducible part of the BZ and generates a starting density for the SCF cycle by a super position of the atomic densities generated before for the free atoms.

In the SCF cycle, the potential constructed from the charge density which used to construct the Hamiltonian used to calculate the eigenvalues and eigenvectors for the valence electrons (valence bands). As a result, a new valence electron density is obtained from the calculated eigenvectors. Then the core states and densities are determined by a fully-relativistic self-consistent calculation. These two charge densities (valence and core) are mixed with the input density to yield a refined input for the next iteration. The simplest mixing scheme is represented by the straight mixing:

$$r_{input}^{i+1} = (1 - Q)\, r_{input}^{i} + Q\, r_{out}^{i} \qquad (2.34)$$

where i refer to the iteration number and Q is the mixing factor.

The self-consistent cycle repeated until convergence is reached, when old and new electron densities are within our computational tolerance.

2.7 Mechanisms used to explain magnetic properties

III-N compounds (eg. AlN) are alloyed by transition metals (eg. Mn) to form magnetic semiconductor compounds; these transition metals have incomplete inner electron orbits. Once they loose their outermost electrons, the remaining electrons in the d-shells have spins pointing in the same direction in order to minimize their energy, and these metals act as magnetic ions.

Zener describes ferromagnetism based on the interaction between the d shells in transition metals. According the Hund's rule the lowest energy for the d-shell occurs when all the energy levels are singly occupied with the spins of electrons pointing in the same direction. Since each electron that has an uncompensated spin carries a magnetic moment of one Bohr magneton, the overall atom will have a finite magnetic moment associated with it.

Mn as an example in this paper has 7 valence electrons and substitutes for a Al atom, 3 of the 7 electrons can replace the 3 Al electrons in the valence band. The remaining 4 electrons have to be put in new localized d-states in the band gap the spin orientation of the electrons in the 3d shells is Mn^{3+} ↑ ↑ ↑ ↑ with total magnetic moment $4\mu_B$. Therefore the electronic structure of transition metal impurities in semiconductors is dominated by d-states in the gap; only the majority states are occupied. The impurity levels are schematically indicated in Figure 2.3 Two different impurity levels have to be distinguished: A two fold degenerate e-state (d_{z2}, d_{x2-y2}), the wave functions of which for symmetry reasons hybridize very little with the valence band p-states, and a three fold degenerate t-state (d_{xy}, d_{yz},d_{zx}) which strongly hybridizes with the p states.

In the neutral configuration only the two e-states and two of the three t-states in the majority band are occupied, while the minority gap states are empty. The Fermi level falls into the majority t-impurity band, such that per Mn atom exactly two e-states and two t-states are occupied, leaving one majority t-state and all minority d-states empty. Therefore the considered system is a half-metallic ferromagnetic, with a moment of $4\mu_B$ per Mn atom.

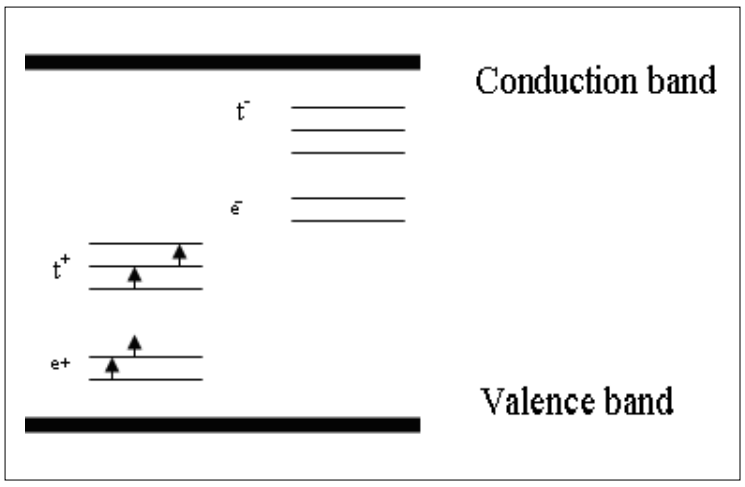

Figure 2.3: Impurity levels of magnetic transition metal impurities in semiconductors: For Mn on the III-site in III-V semiconductors the double degenerate e+ state and two of the three degenerate t+ states are occupied.

Different mechanisms are used to explain magnetic properties of semiconductors.

2.7.1 Zener Model (Mean Field Theory)

The Zener [72] model, based on the mean field theory, states that ferromagnetism occurs through the interactions of the spins of the localized magnetic ions. The electrons in the incomplete d shells tend to

gain the lowest energy state by align electrons spin parallel, or have the highest possible net spin to attain.

The interaction between the d shells of adjacent atoms has always the same sign and in all circumstances lead to an antiferromagnetic coupling. On the other hand, the spin of an incomplete shell is always strongly couples to the conduction electrons.This coupling tends to align the spins of the incomplete shells in a ferromagnetic manner. The competition between these two tendencies determines the magnetic state of the material.

2.7.2 Double Exchange Mechanism

In the double exchange mechanism which was originally proposed by Zener, magnetic ions in different charge states couple with each other by virtual hopping of the “extra” electron from one ion to another. If the neighboring magnetic moments of the transition metal ions are in the same direction, the 3d band is widened by the hybridization between the spin-up states Figure 2.4. The band energy in the ferromagnetic configuration is lowered by introducing carriers in the d-band. In this case, the partially filled 3d bands of the transition metal ions facilitates hopping of carriers from one ions orbital to another, provided that the spins of the hopping electrons’ spins are in the same direction. Consequently, the electrons lower their kinetic energy by hopping in the ferromagnetic state. This is the so-called double exchange mechanism.

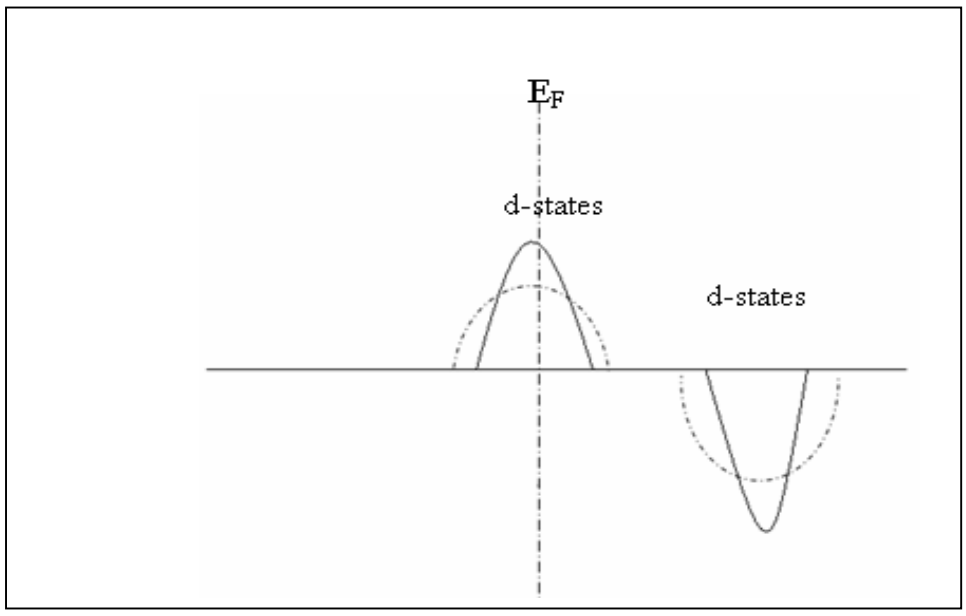

Figure 2.4: Double exchange: Due to the broadening of the impurity t-band with increasing Mn concentration x, states are transferred to lower energies, leading to an energy gain, if the Fermi energy lies in the band.

2.7.3 Direct Superexchange

The direct superexchange mechanism is observed in substances in which magnetic ions are separated by an intervening non magnetic ion [73]. The interaction between the wave functions of the magnetic ion's electrons is antiferromagnetic and therefore aligns the neighboring Mn ions antiferromagnetically. This type of interaction usually opposes ferromagnetic properties in DMS materials and becomes more pronounced as the Mn concentration is increased.

Chapter three

Computational details

3.1 Introduction

For the binary compounds AlN and MnN the muffin-tin radii (R_{MT}) values chosen are 1.8 Bohr for Al and Mn; and 1.6 Bohr for N. The K-integration over the Brillouin zone is performed with the Monk horst pack [75] scheme. The number of K-points in the irreducible Brillouin zone for the binary alloys is 512. The iteration process is repeated until the calculated total energy of the crystal converges to less than 10^{-5} Ry. Basis functions, charge density and potential are expanded inside the muffin-tin spheres in combination with spherical harmonic functions with a cut-off l_{max} = 10, and in Fourier series in the interstitial region. Moreover, we use a parameter $R_{MT}K_{max}$ = 8, which determines matrix size (convergence), where K_{max} is the plane wave cut-off and RMT is the smallest of all atomic sphere radii.

3.2 Zincblende (Cubic Zinc Sulfide) Structure

Compounds with zincblende structure ZB crystallize in a cubic conventional cell which composed of two fcc structures displaces from each other by one-quarter of a body diagonal. Eight atoms in each one, in this present work Al or Mn atoms are placed on one fcc lattice coordinates and N atoms on the other fcc lattice. The coordinates for Al or Mn atoms are (0, 0, 0) a, (0, 0.5, 0.5) a, (0.5, 0, 0.5) a, (0.5, 0.5, 0) a, while the coordinates for N atoms are (0.25, 0.25, 0.25) a, (0.25, 0.75, 0.75) a, (0.75, 0.25, 0.75) a, (0.75, 0.75, 0.25) a, where a is the lattice parameter [**96**]. If we take MnN as an example Figure 3.1, each N atom is surrounding by four equally distance Mn atoms and vice versa. One of the

most famous compounds is ZB compounds is Zinc Sulfide The space group is F34_m and the primitive vectors of fcc are:

$$\mathbf{r}_{a_1} = \frac{a}{2}\hat{j} + \frac{a}{2}\hat{k} \quad , \qquad \mathbf{r}_{a_2} = \frac{a}{2}\hat{i} + \frac{a}{2}\hat{k} \quad , \qquad \mathbf{r}_{a_3} = \frac{a}{2}\hat{i} + \frac{a}{2}\hat{j}$$

Alloys consist of a cation sublattice, where metals are interchanged (Al by Mn) and of an anion sublattice (N), as shown in Figure 3.1, both originated from the zincblende structure.

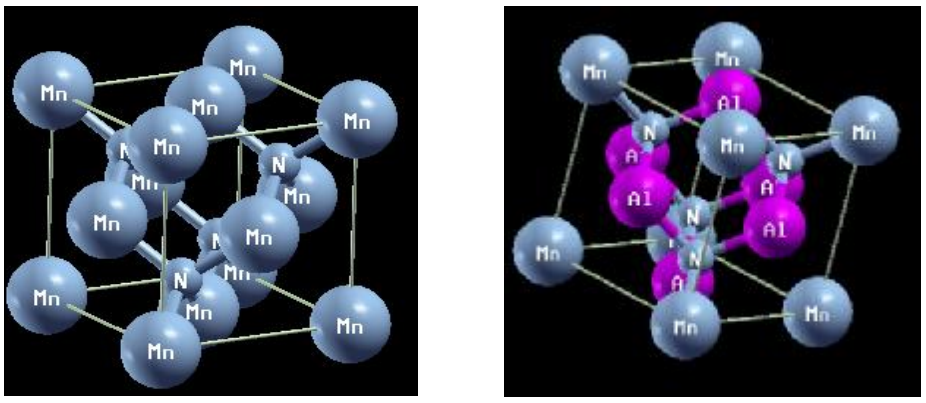

(a) (b)

Figure 3.1: Unit cell used to simulate the $Al_{x-1}Mn_xN$ (a) with x=1, (b) with x=0.25.

3.3 Choosing $R_{MT}K_{max}$ and the number of K-points

In order to achieve the energy eigen value convergence, the wave function in the interstitial region is expanded in terms of plane waves, with a cutoff of $R_{MT}K_{max}$ (where K_{max} is the maximum value for the reciprocal lattice vector K, and R_{MT} is the average radius of the MT spheres). Calculating the bulk properties for the binary and ternary alloys must be made after applying some tests. K-points and Energy cutoff tests are very important procedures to get best results in short time.

Choosing $R_{MT}K_{max}$ in this test we make a number of sessions with the same number of K- points, same R_{MT} for all sessions, the same $\boldsymbol{l_{max}}$

and the same lattice parameter. We make a run for every session and looking for the energy. Finally we choose the $R_{MT}K_{max}$ which makes the structure more stable, in other words we look for the $R_{MT}K_{max}$ with a minimum energy. As an example Table 3.1 show us that the best $R_{MT}K_{max}$ for $Al_{0.75}Mn_{0.25}N$ is $R_{MT}K_{max}$ =8.

Table 3.1: Test to find the best R_{MT}Kmax for $Al_{0.75}Mn_{0.25}N$.

No.	$R_{MT}K_{max}$	E_{total}(total energy in Ry units)
1	6	-4212.772349
2	6.5	-4212.83084
3	7	-4212.85841
4	7.5	-4212.868423
5	8	-4212.878512
6	8.5	-4212.876816
7	9	-4212.865295

To choose the best number of K-points we must make the same steps for choosing the best $R_{MT}K_{max}$, in this test we must fix all parameters (lattice parameter, $R_{MT}K_{max}$, $\boldsymbol{l_{max}}$ and the same R_{MT}) except number of K-points.Table 3.2 shows us the test results for $Al_{0.75}Mn_{0.25}N$.

Table 3.2: Choosing K-points for $Al_{0.75}Mn_{0.25}N$.

No.	K-points	K-reduced	Matrix	E_{total}(in Ry)
1	27	5	3X3X3	-4212.818035
2	64	8	4X4X4	-4212.855674
3	125	14	5X5X5	-4212.856816
4	216	20	6X6X6	-4212.857024
5	343	30	7X7X7	-4212.857692
6	512	40	8X8X8	-4212.856654
7	729	55	9X9X9	-4212.856608
8	1000	70	10X10X10	-4212.856725

In order to simulate the ordered zincblende structure with 25%, 50% and 75% concentrations of Mn, we consider a model based on an eight atoms supercell with cubic symmetry.The core states for Al, Mn and N are treated self consistently and fully relativistically relaxed in a spherical approximation; while the valence states are treated self consistently within a semi-relativistic approximation (spin–orbit effects are not included).

Basis functions, charge density and potential are expanded inside the muffin-tin spheres in combination with spherical harmonic functions with a cut-off l_{max} = 8 for each concentration (25%, 50% and 75% of Mn) as in the binary study, and in Fourier series in the interstitial region.

Moreover, we use a parameter $R_{MT}K_{max}$ = 8 for each concentration (25%, 50% and 75% of Mn), where K_{max} is the plane wave cut-off and RMT is the smallest of all atomic sphere radii.The R_{MT} for the $Al_{1-x}Mn_xN$ (with x= 0.25, 0.5, 0.75) compound were chosen to be 1.78 Bohr for Al and Mn atoms, and 1.6 Bohr for N atom. The number of K-pointes in the irreducible Brillouin zone is 343 for 0.25%, 0.5% and 0.75% concentrations, which correspond to 7X7X7 k-mesh. We chose this number of k-pointes after the test on the best number of k-pointes as mentioned before. The iteration process is repeated until the calculated total energy of the crystal converges to less than 10^{-5} Ry.

3.4 Optimization

One of the most important steps is the optimization; it’s the first step in our work (before the usual tests for the best k-pointes and $R_{MT}K_{max}$) and in every work. By optimization we can determine the equilibrium lattice parameter $a_\circ$, bulk modulus ***B***, bulk modulus derivative ***B'***, energy $E_\circ$ and volume $V_\circ$ at equilibrium.

The structural properties in the strain-free case are obtained by a minimization of the total energy depending on the volume for $Al_{1-x}Mn_xN$ and the binary compounds (MnN and AlN) in the zincblende structure, by using a trial value (usually experimental one for the binary and from this relation, $a_{(Al_{1-x}Mn_xN)} = (x)\, a_{(MnN)} + (1-x)\, a_{(AlN)}$, for the ternary alloys) of the lattice constants and then fitting the total energy versus volume according to the Murnghan's equation of state [80]. We compute the equilibrium lattice constants, bulk modulus and pressure derivative of the bulk modulus.

$$E(V) = E_{\circ}(V) + \frac{BV}{B^{/}(B^{/}-1)}\left[B\left(1-\frac{V_{\circ}}{V}\right)+\left(\frac{V_{\circ}}{V}\right)^{B^{/}}-1\right] \qquad (4.1)$$

where E_o and V_o are the energy and volume at equilibrium, B and B' are the bulk modulus and its derivative.

The volume of the unit cell MnN or AlN is $V_o = a_o^3/4$, (four molecules per primitive cell), so the equilibrium lattice constant (a_o) can be calculated as $a_o = (4V_o)^{1/3}$. The volume of the unit cell for $Al_{1-x}Mn_xN$ is $V_o = a_o^3$, so $a_o = V_o^{1/3}$. From this we can compute (a_o) for each concentration of Mn.

In the next chapter we present the calculated bulk properties, a_o, E_o, V_o, B and B', of the binary compounds AlN and MnN as well as the ternary alloys $Al_{1-x}Mn_xN$ (x=0.25, 0.5 and 0.75). Also we present the magnetic results for MnN compound and the ternary alloys $Al_{1-x}Mn_xN$.

Chapter four

Results and Discussions

4.1 Introduction

This charter is devoted to the principle results of the scalar relativistic full-potential linearized augmented plane wave plus local orbitals (FP-L/APW+lo) [47] approach based on the density functional theory [49] within the LSDA and GGA approximations using scheme of Perdew, Brouke and Ernzerhof [50]. We adopt the Ceperley-Alder [61] form for exchange-correlation energy as parameterized by Perdew and Wang [74]. In the present calculations we apply the recent version of Wien package WIEN2K **[**77**,** 78**]**. APW+lo is used inside the atomic sphere for chemically important *l*-orbitals that are difficultly converge (p,d or f orbitals) **[**79-81**]**. For all other partial waves the LAPW scheme is used.

Spherical harmonics expansion is used inside the non-overlapping spheres of muffin-tin (MT) radius (R_{MT}), for the remaining space of the unit cell the plane wave basis is used. The MT radius values chosen for the binary compounds AlN and MnN are 1.8, 1.6 Bohr for (Al, Mn) and N respectively.The maximum ***l*** value for the wave function expansion inside the atomic spheres was confined to $\boldsymbol{l_{max}}$=10. In order to achieve the energy eigenvalue convergence, the wave function in the interstitial region is expanded in terms of plane waves, with a cutoff of $R_{MT}K_{max}$=8 (where K_{max} is the maximum modulus for the reciprocal lattice vector, and R_{MT} is the average radius of the MT spheres). The number of K-points in the irreducible Brillouin zone is 512 for the binary compounds AlN and MnN which correspond to 8X8X8 k-mesh which reduced to 43 k-points. We chose this number of k-points after the test on the best number of k-points

as mentioned before, the total energy and eigenvalues were converged to 10^{-5}eV.The calculations were performed with spin-polarized potentials in order to analyze the ferromagnetic phases of the compounds.
Calculations are performed on AlN, MnN compounds and $Al_xMn_{1-x}N$ (x= 0.25, 0.5, 0.75).

In part I we study the structural, electronic and magnetic properties of AlN and MnN compounds. In part II, we studied the effect of manganese (Mn) doping on AlN compound and determine the principal characteristics of diluted magnetic semiconductors $Al_{1-x}Mn_xN$ with (x= 0.25, 0.5, 0.75) in their ferromagnetic phase.

Part I:

4. I.1: Cubic binary compounds MnN and AlN.

We report the calculations of electronic structures of the binary compounds MnN and AlN in the zincblende phase. We use the theoretical local spin density approximation (LSDA) and the generalized gradient approximation (GGA) within density functional theory.

4. I.2: Optimization

The structural properties in the strain-free case are obtained by a minimization of the total energy depending on the volume for MnN and AlN in the zincblende structure by fitting the total energy versus volume according to the Murnghan's equation of state [80], equation (3.1).
We compute the equilibrium lattice constants, bulk modulus and pressure derivative of the bulk modulus. Figure 4.I.1 and Figure (4.I.2) show the total energy as a function of the unit cell volume for MnN and AlN within GGA and LSDA approaches.

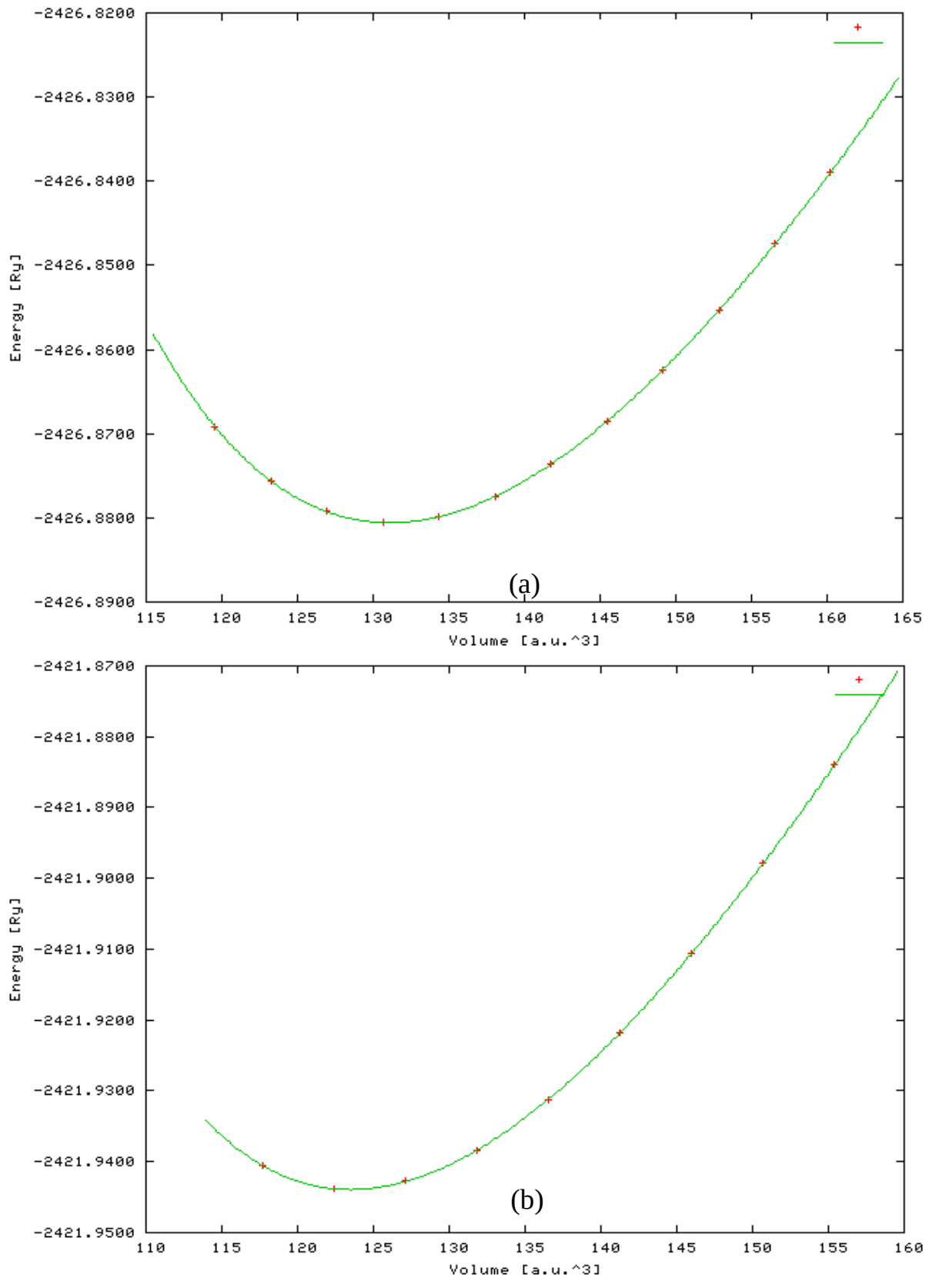

Figure 4.I.1: Total energy as a function of the volume for the zincblende MnN using a) GGA, b) LSDA methods.

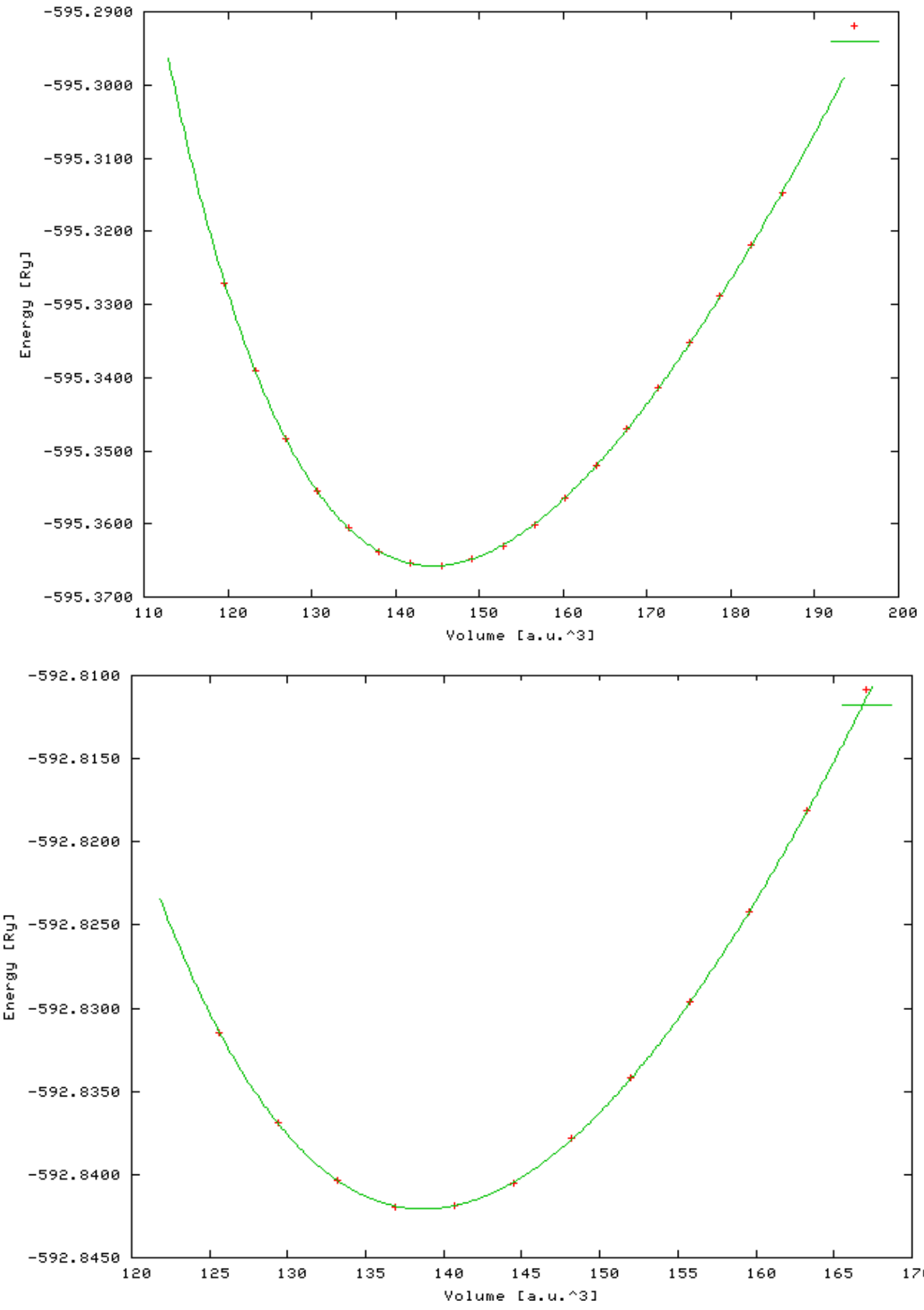

Figure 4.I.2: Total energy as a function of the volume for the zincblende AlN using a) GGA, b) LSDA methods.

We can see that the GGA total energy ($E_\circ$) is less than the LSDA approach for both MnN and AlN. For MnN, $E_\circ$ = -2426.88Ry with GGA method and $E_\circ$= -2421.94Ry with LSDA method.For AlN, $E_\circ$= -595.36Ry with GGA method and $E_\circ$= -521.84 Ry with LSDA method. This means that the GGA is more accurate thane the LSDA approximation.

We computed the equilibrium lattice constant (a_o).For MnN, it is found that the minimum energy occurs at a lattice constant $a_\circ$ = 4.27A° and 4.184 A° by GGA and LSDA methods respectively. The lattice constants have been found by GGA and LSDA methods for AlN are 4.409A° and 4.348A° respectively.

In table (4.I.1) the equilibrium lattice constant, bulk modulus and pressure derivative of the bulk modulus for MnN are shown.

Table 4.I.1: Equilibrium lattice constant a, bulk modulus *B* and pressure derivative of the bulk modulus ***B'***for MnN compound in zincblende structure.

Structural Parameters	Present LSDA	Present GGA	Other Calculations LSDA	Other Calculations GGA
$a_\circ(A^\circ)$	4.184	4.278	4.19[a],4.187[b]	4.3[a], 4.309[b]
$B_\circ(Gpa)$	338.2	274.5	336[a], 329.6[b]	271[a], 273.2[b]
B'	4.926	4.8104	4.948[b]	4.4997[b]

[a]Ref.[82], [b]Ref.[83]

From table 4.I.1, the obtained lattice parameters are larger for the GGA approach than the LSDA approach. The difference between the two

approaches is about 0.095A°. On the contrary, the GGA values for the bulk modulus are smaller than the LSDA values. The results are very close to and agree with the other results.

Table 4.I.2 summarizes the results of structure optimization for zincblende AlN calculations.

Table 4.I. 2: Lattice constant a, bulk modulus ***B***, and pressure derivative of the bulk modulus ***B'***of the zincblende AlN.

Structural Parameters	Present		Other Calculations		Experiment
	LSDA	GGA	LSDA	GGA	
a_o(A°)	4.348	4.409	4.31-4.376[a]	4.39-4.42[b]	4.37[c]
B(GPa)	210.74	192.89	211.78-216[a]	191-193.3[b]	----
B'	3.923	3.792	3.2-3.9[a]	3.8-3.81[b]	----

[a]Ref. [46, 84, 85, 86, 87], [b]Ref. [84, 85, 86], [c]Ref. Wurtzite structure Ref. [88]

Our calculations show that the GGA lattice constant is greater than the LSDA of about 0.06A°, while the bulk modulus value obtained by GGA method is smaller than which obtained by LSDA method of about 18Gpa. Lattice constant obtained from LSDA approximation is smaller than the experimental value by 0.022A°, while GGA calculation greater than experimental value by 0.039A°.

4. I.3 MnN Band structure

Band gap is very important for determining the electronic and magnetic properties of the compounds or alloys. As an example, by calculating the band gap we can determine whether the compound is metal, semimetal, semiconductor or insulator. After the optimization and calculating the exact structural parameters we build a new structure with

the equilibrium lattice parameters to plot the band structure from which the nature of the band gap and its width was calculated.

Figures 4.I.3 (a-f) show the dependent of the majority-spin system as a function of the lattice parameter of MnN compound. As the lattice parameter is varied the majority-spin system keeps a metallic character in which the Fermi energy lies in the band, while the minority-spin, Figures 4.I.4 (a-f), evolves from a metallic character in which the Fermi energy lies in the band to insulating character in which the Fermi level lies in the gap with an energy gap = 2.712 eV. This behavior may be understood on the basis of a model of charge transfer from Mn-3d to N-2p shells.

MnN may be half-metallic in the zincblende stretched lattices in which a> 4.91A$^{\circ}$ (half-metals are defined by an electronic structure, which shows conduction by charge carriers of one spin direction exclusively), therefore showing conduction by charge carriers of one spin direction.

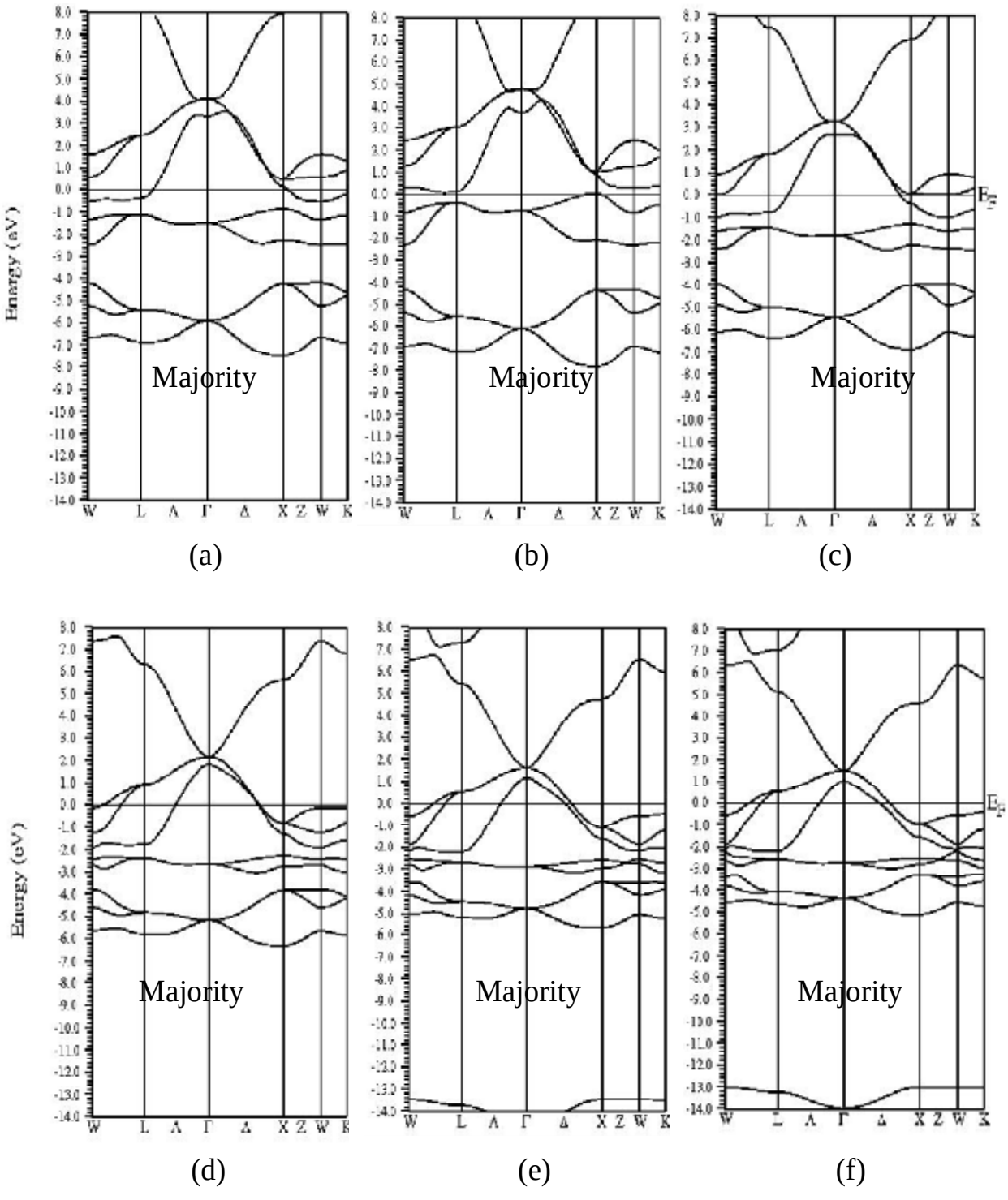

Figures 4.I.3 (a-f): The evolution of the majority band structures as a function of the lattice parameter of MnN compound using GGA method. Lattice constant a= 4.18 A°, 4.279A°, 4.445 A°, 4.656 A°, 4.868A° and 4.998A° are shown in Figures a, b, c, d, e, and f respectively.

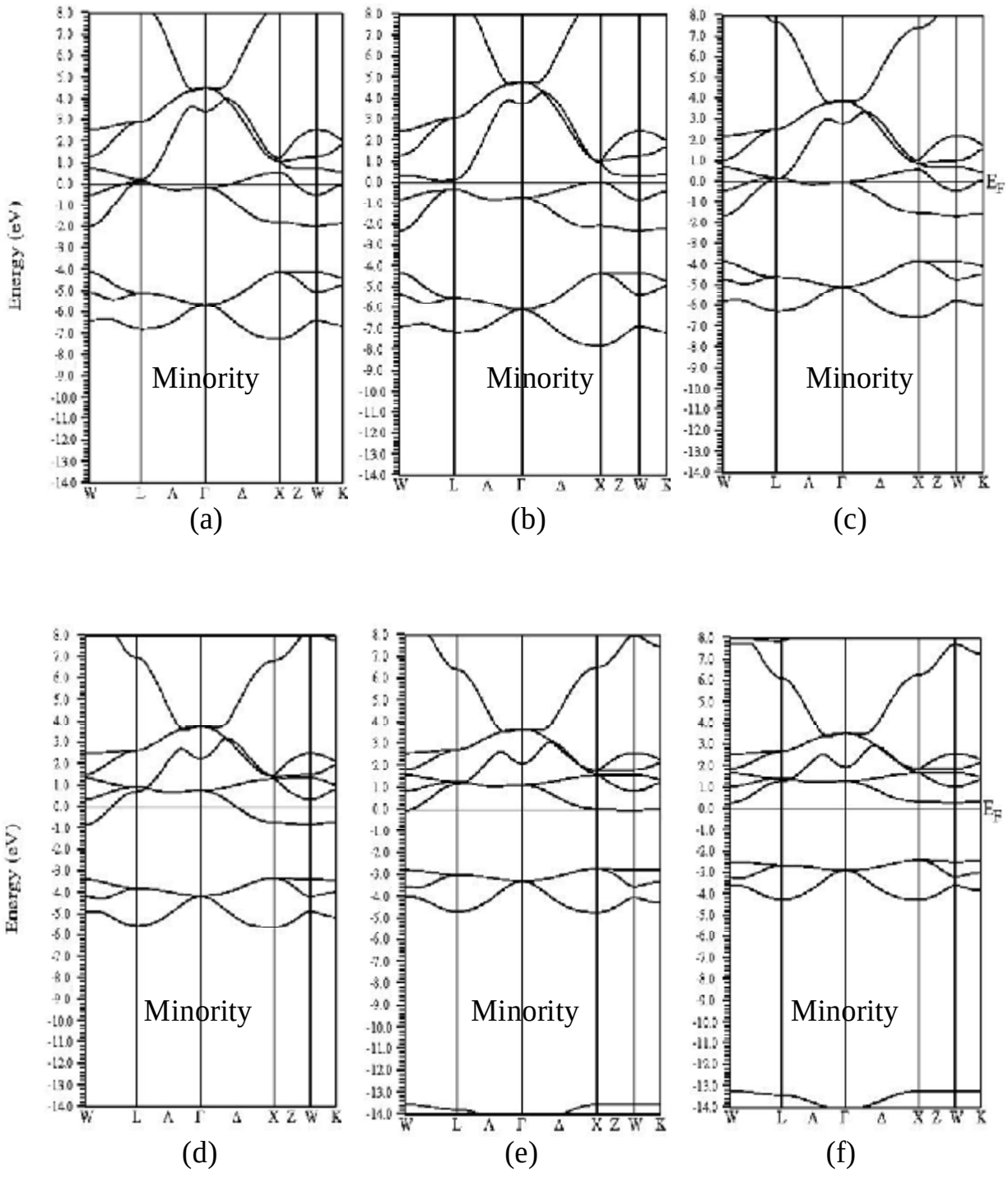

Figures 4.I.4 (a-f): The evolution of the minority band structures as a function of the lattice parameter of MnN compound using GGA method. Lattice constant a= 4.18 A°, 4.279A°, 4.445 A°, 4.656 A°, 4.868A° and 4.998A° are shown in Figures a, b, c, d, e, and f respectively.

Present calculations shows that the magnetic moments for MnN are zero at the equilibrium lattice constant $a_\circ$ =4.184A$^\circ$ using LSDA method, and it is equal to 0.67μ_B using GGA method at $a_\circ$ =4.27A$^\circ$, part of this difference related to the increment in the lattice constant with GGA approximation.

Fig 4.I.5 shows that the magnetization increases as the lattice parameters increases and tend to saturate at the value 4μ_B in both LSDA and GGA approaches. It is noticeable that the LSDA values always tend to be lower than the GGA ones; GGA method is more efficient to calculate the magnetic moment because it adds the gradient term to the form of Exchange-correlation energy. One can see that as the material lattice expansion goes from paramagnetic to ferromagnetic phase. The saturation of the magnetization at the value 4 μ_B may be understood on the basis of a model of charge transfer from Mn-3d to the neighbors N-2p shells [89]. This charge transfer is not complete due to the strong interaction originating from the p-d hybridization. The hybridization is reduced as the lattice constant increase and so reaches to a magnetic moment of 4 μ_B.

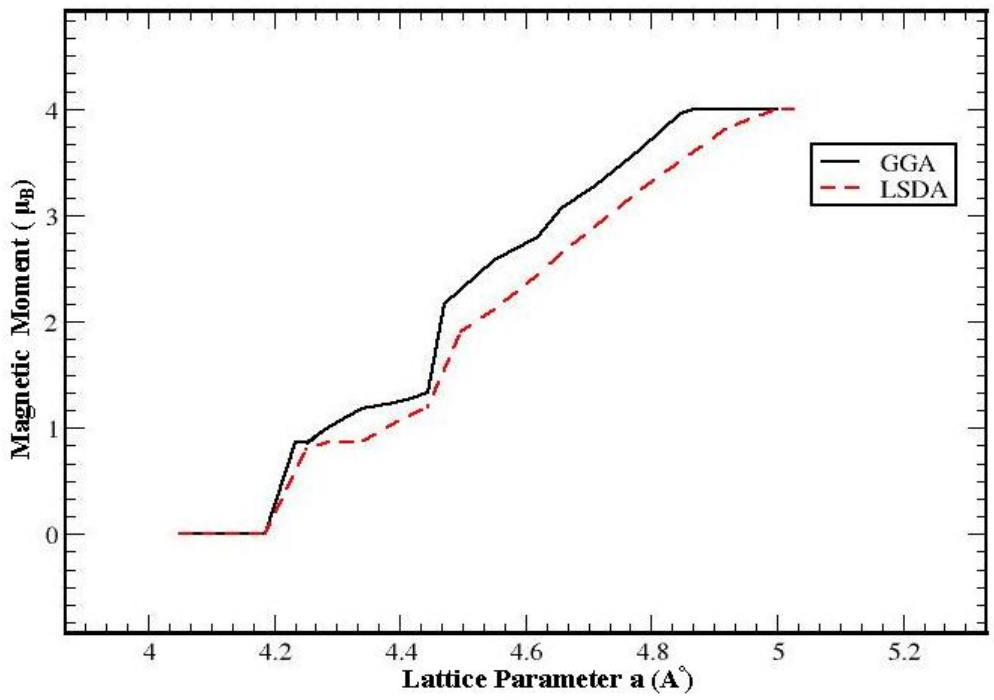

Figure 4.I.5: Magnetization per unit cell for the MnN compound as a function of the lattice parameter in both LSDA and GGA approaches.

4. I.4 AlN Band structure.

Fig 4.I.5 shows the band structures along the symmetry line for zincblende AlN using LSDA and GGA approaches. The band structures are calculated at the equilibrium lattice constant for both LSDA and GGA approaches. There are a slight difference between LSDA and GGA, and this is related to the slight difference between the lattice constants where the GGA lattice constant is slightly greater thane LSDA, the difference is about 0.061 A°.

The band gap for AlN is indirect; it is between the Γ point (the valence-band maximum) and the X point (the conduction-band minimum) therefore it is a Γ-X indirect band gap. The indirect band-gap is 3.258eV

and 3.278eV using LSDA and GGA approaches respectively, Kanoun *et al* [46] used FP-LAPW +lo in his calculations, the predicted Γ-X indirect band gap was 3.211eV and 3.304eV using LSDA and GGA approaches respectively. So present calculations are in good agreement with Kanoun *et al* [46] calculations.

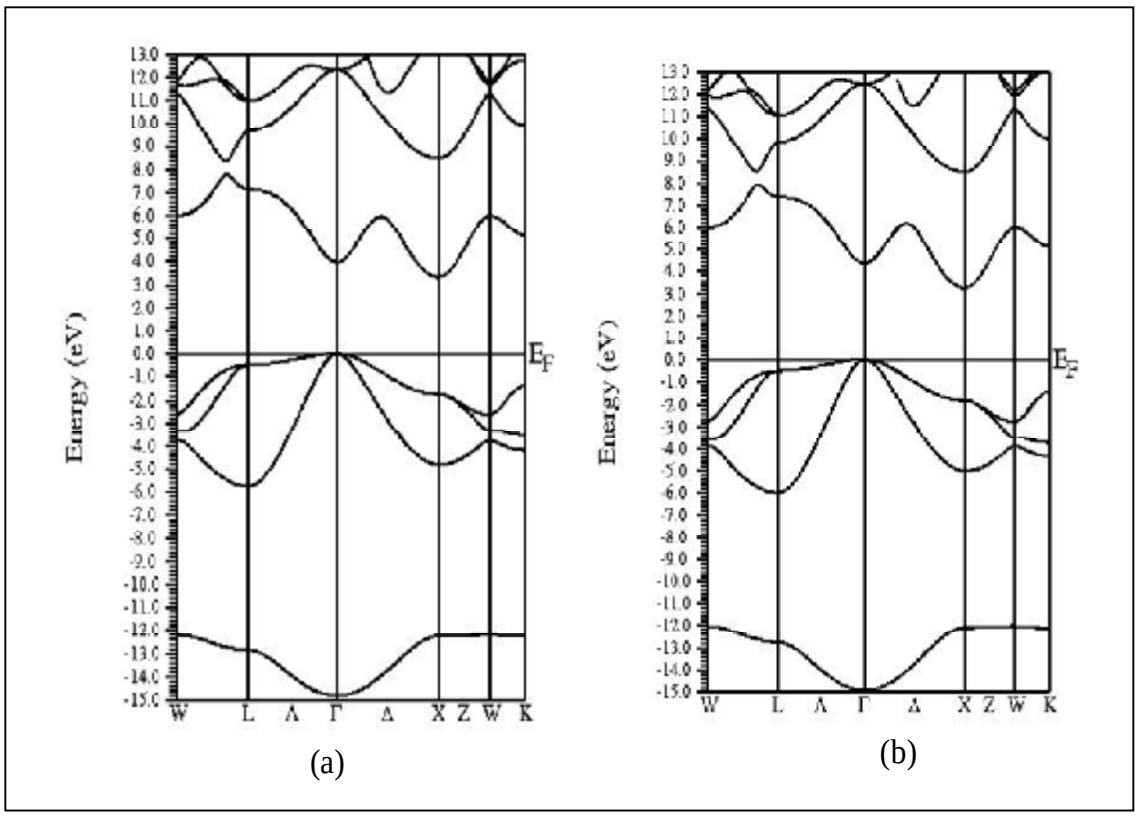

Figure 4.I.6: The band structures for zincblende (ZB) AlN along the symmetry line with a) GGA, b) LSDA approaches.

In Figure 4.I.6 and Figure 4.I.7 we show the calculated total and partial density of states (DOS) for AlN ; density of state of a system describes the number of states at each energy level that are available to be occupied. In the total density of state the lower part of the valence band dominate by N 2s, the upper part of the valence dominate by N 2p and a small value from Al 2p. From the partial DOSs we can see the

hybridization of N 2p with the Al s and p states; also we can see the forbidden region (energy gap) and the Fermi energy lie in its lower edge.

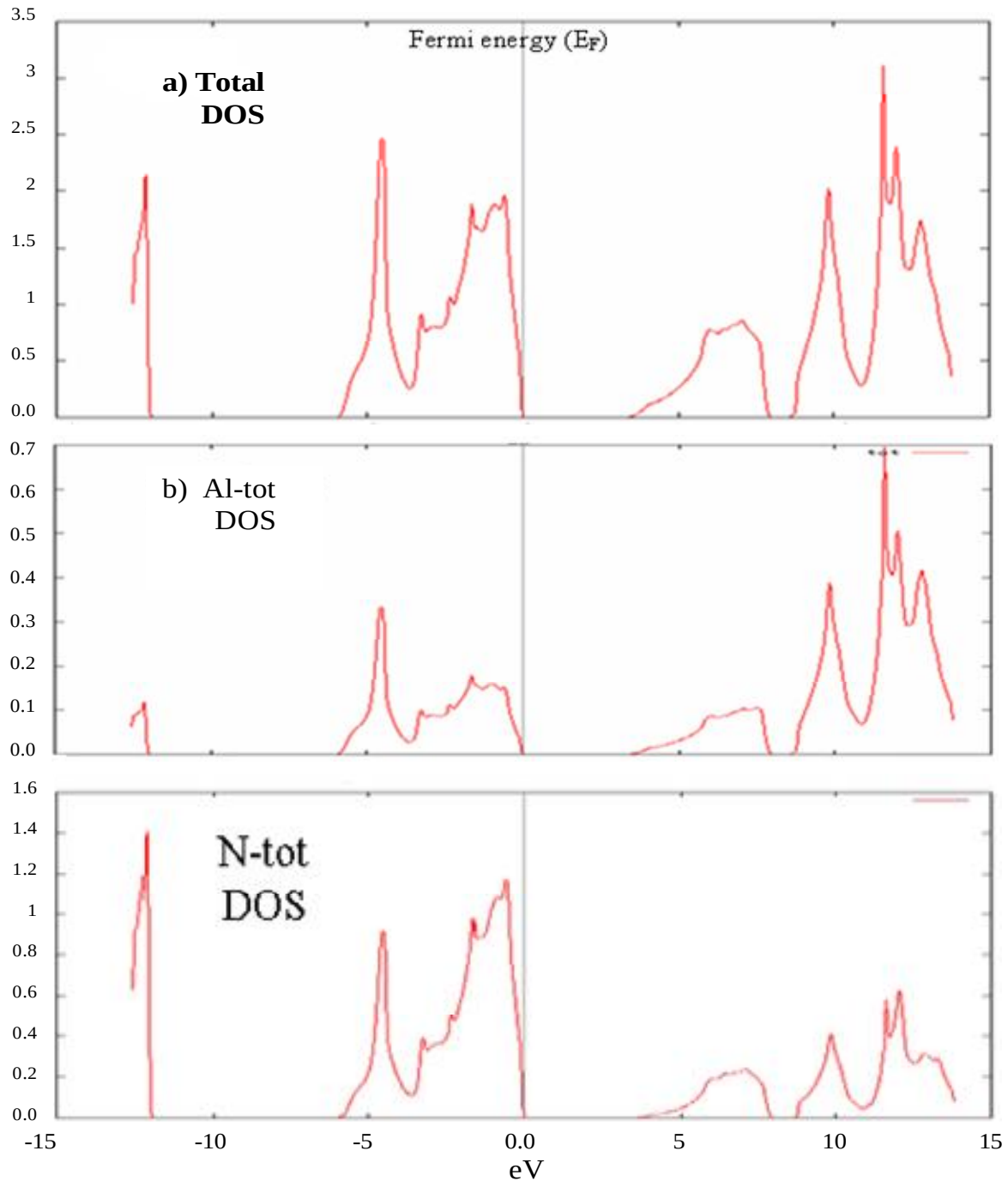

Figure (4.I.7): a) Total density of states of AlN. b) Total density of states of Al atom. c) Total density of states of N atom.

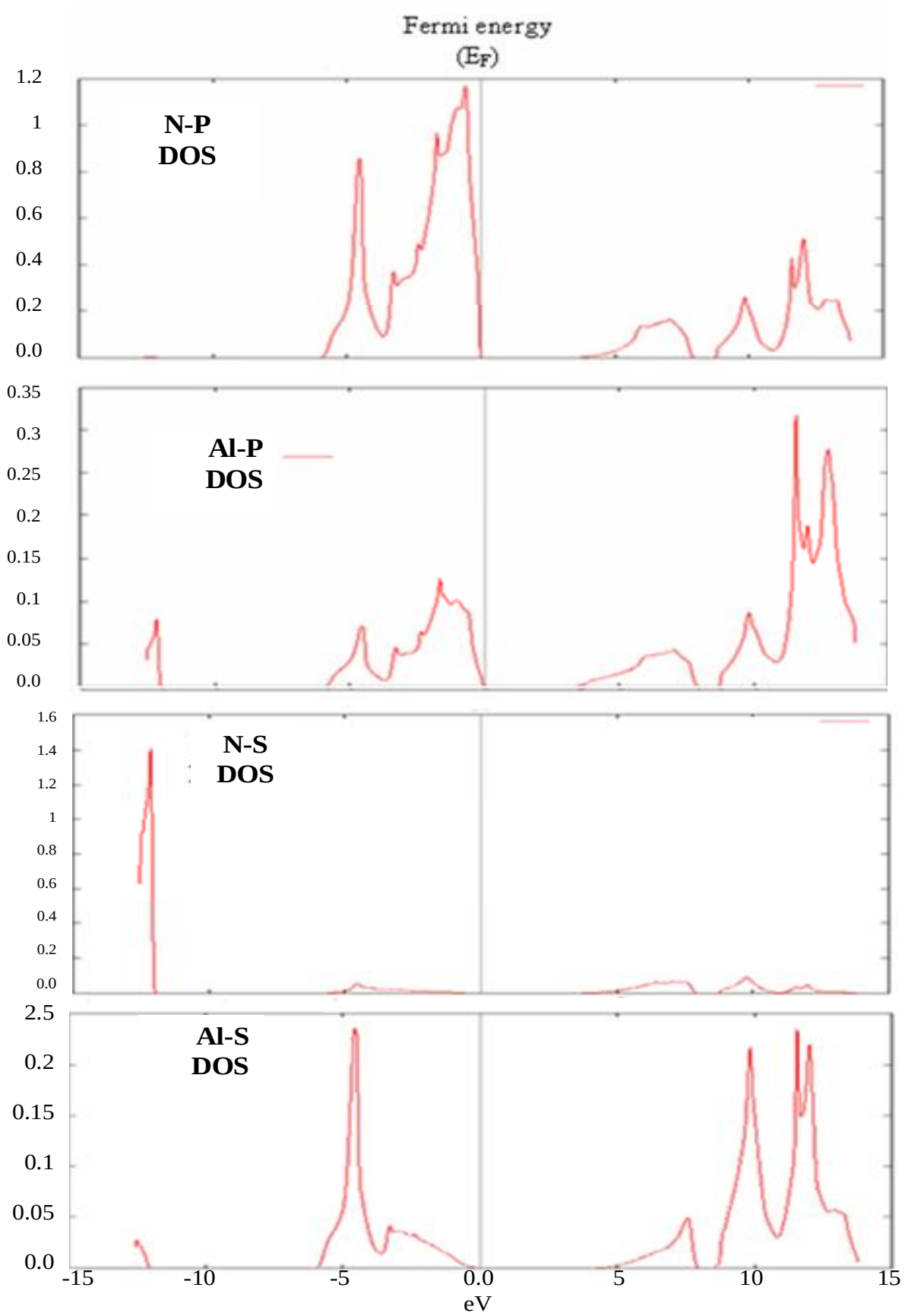

Figure (4.I.8): partial density of states DOS for AlN in zincblende (ZB) system.

Part II

4. II: Manganese (Mn) doping on AlN ($Al_{1-x}Mn_xN$)

For $Al_{1-x}Mn_xN$ alloys calculations the muffin-tin radius values are chosen to be (1.78) Bohr for both Aluminum and Manganese atoms (Al, Mn) and 1.6 Bohr for Nitrogen atom (N). Charge density and potential are expanded inside the muffin-tin spheres in combination with spherical harmonic functions with a cut-off $\boldsymbol{l}_{max}$=10, and in Fourier series in the interstitial region.

In order to achieve the energy eigenvalues convergence, the wave function in the interstitial region is expanded in terms of plane waves, with a cutoff of $R_{MT}K_{max}$=8 (where K_{max} is the maximum modulus for the reciprocal lattice vector, and R_{MT} is the average radius of the MT spheres). The number of K-points in the irreducible Brillouin zone is 343 for 0.25%, 0.5% and 0.75% concentrations which correspond to 7X7X7 k-mesh. The total energy and eigen-values were converged to 10^{-5}eV. The calculations were performed with spin-polarized potentials in order to analyze the ferromagnetic phases of the compounds.

4. II.1: Structural optimization

The total energy of $Al_{1-x}Mn_xN$ has been calculated as a function of the global volume. The equilibrium lattice parameters, bulk modulus and it's pressure derivative following from a fit of the total energy as a function of the volume to the Murnagahn equation of state [**76**] (Figure 4.II.1 for x=0.25 with LSDA and GGA methods, Figure 4.II.2 for x=0.5, and Figure 4.II.3 for x= 0.75).

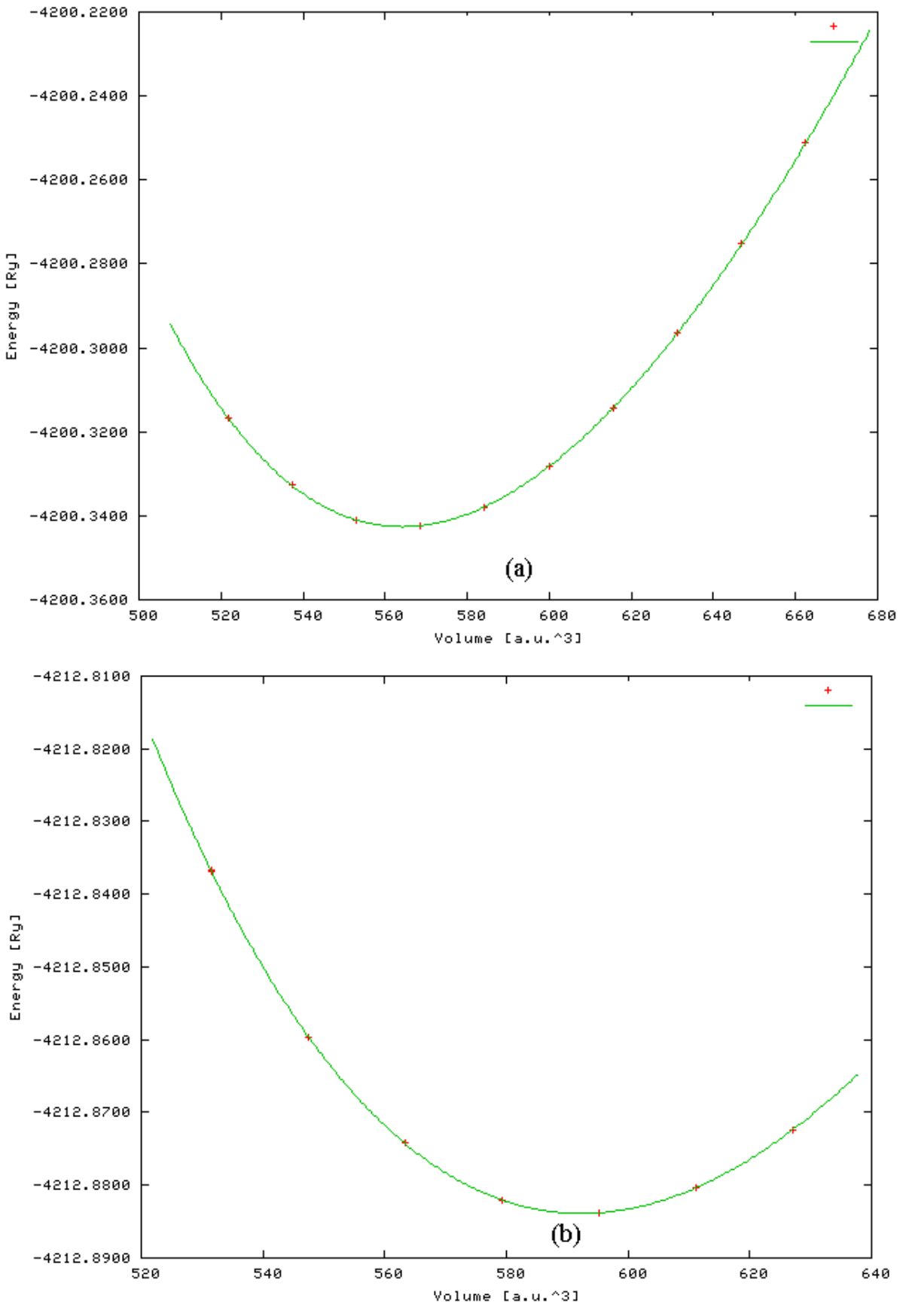

Figure 4.II.1: Total energy as a function of the volume for the zincblende $Al_{0.75}Mn_{0.25}N$ with approximations: a) LSDA b) GGA.

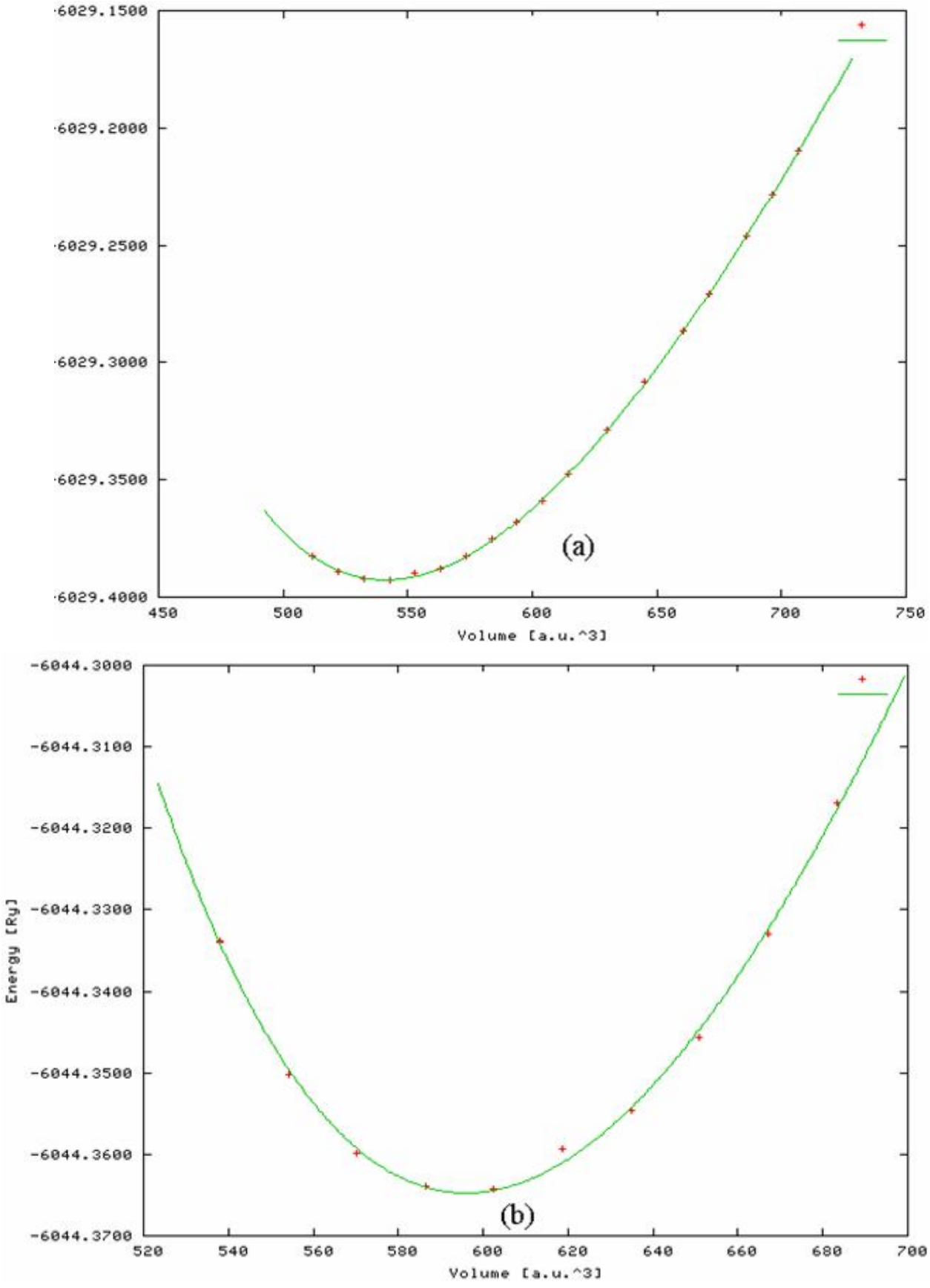

Figure 4.II.2: Total energy as a function of the volume for the zincblende $Al_{0.5}Mn_{0.5}N$ with approximations: a) LSDA, b) GGA.

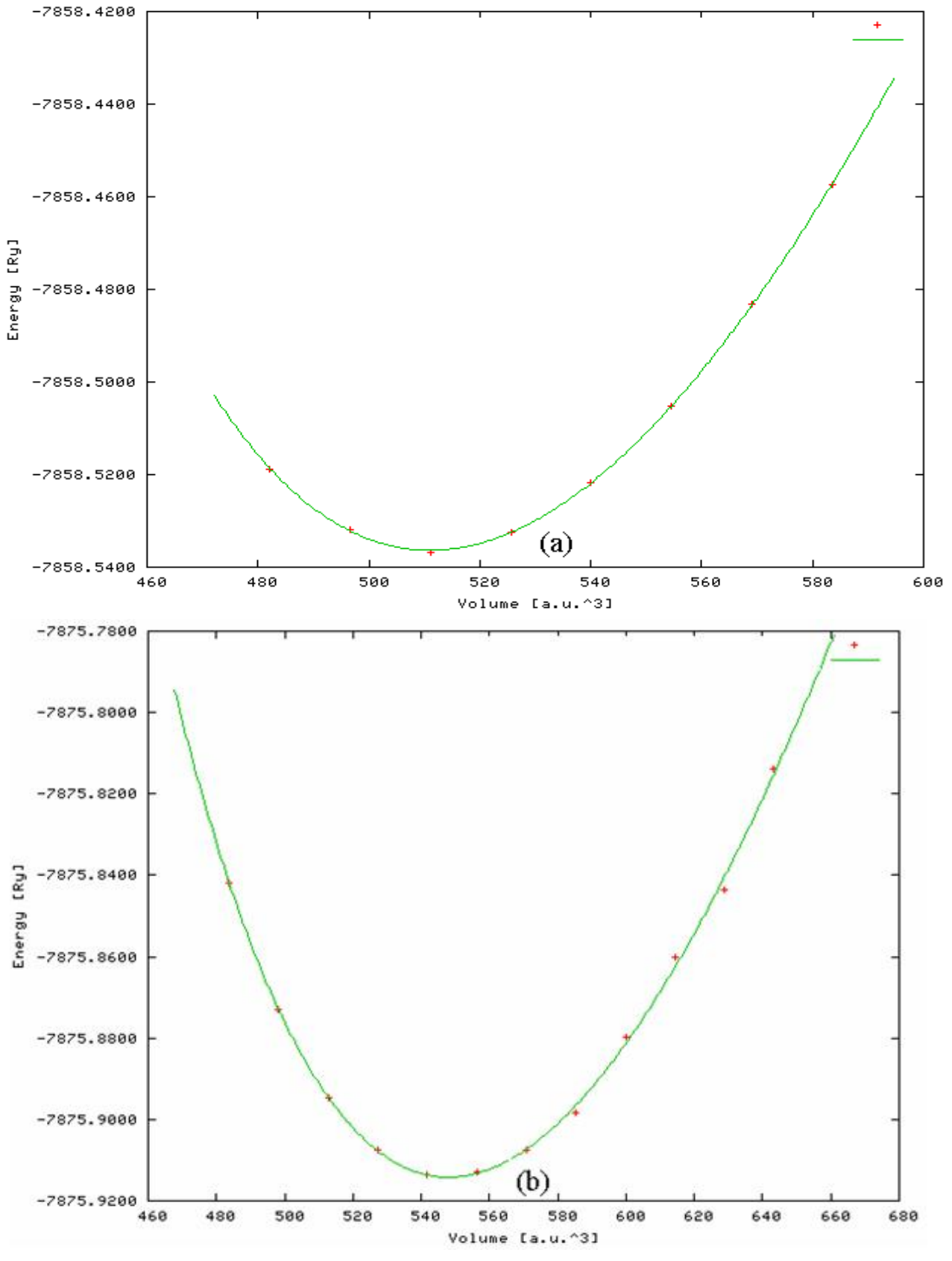

Figure 4.II.3: Total energy as a function of the volume for the zincblende $Al_{0.25}Mn_{0.75}N$ with approximations: a) LSDA, b) GGA.

We can see in table 4.II.1 that the energy $E_\circ$ at equilibrium lattice constant using LSDA method always is less than GGA method, this is related to the modification in calculation Exchange-correlation energy with GGA by adding the gradient to its form. This means that these compounds are more stable with GGA approximation.

Table 4.II.1: Energy $E_\circ$ (Ry) for $Al_{1-x}Mn_xN$ (x=0.0, 0.25, 0.5, 0.75 1.0), using LSDA and GGA approximations.

	LSDA	GGA	Concentration
Energy ($E_\circ$) in (Ry) units	**-592.845063**	**-595.365738**	**0.0**
	-4200.342598	**-4212.883878**	**0.25**
	-6029.392610	**-6044.364744**	**0.5**
	-7858.536347	**-7875.91419**	**0.75**
	-2421.934262	**-2426.880581**	**1**

Also we can see from table 4.II.1 that the alloys ground state energys ($E_\circ$) is smaller than $E_\circ$ for the binary MnN and AlN, that's because the alloys are ferromagnetic but the binary are not. When the electrons are in the ferromagnetic state the energy decrease and are more stable.

Table 4.II.2 shows the predicted values of the structural parameters for the concentration x=0.25, the results are compared with the binary compound AlN shown in table 4.I.2 and are found in the same order. This is related to the low concentration of Mn atom with x=0.25. We can see that the equilibrium lattice constant with GGA method is greater than the LSDA method of about 0.144A°.

Table 4.II.2:- Lattice constant $a_\circ$, bulk modulus ***B***, and pressure derivative of the bulk modulus ***B'*** for the zincblende $Al_{0.75}Mn_{0.25}N$.

Structural Parameters	Present		Other Calculations	
	LSDA	GGA	LSDA	GGA
$a_\circ$(A°)	4.37258	4.444147	4.3726[a]	-----
***B*(GPa)**	206.68	183.0881	208.5[a]	-----
B'	4.278	4.156	3.74[a]	------

[a]Ref [46].

On the other hand bulk modulus ***B*** and pressure derivatives of the bulk modulus ***B'*** are greater with LSDA. The results as shown in table 4.II.2 are in an excellent agreement with the other calculations which are done by using FP-LAPW + lo method [46].

Table 4.II.3shows the predicted values of the structural parameters for the other two concentrations x=0.5 and 0.75.

Table 4.II.3: Lattice constants $a_\circ$, bulk modulus *B*, and pressure derivatives of the bulk modulus ***B'*** of the zincblende $Al_{0.\ 5}Mn_{0.\ 5}N$, $Al_{0.\ 25}Mn_{0.\ 75}N$.

Structural Parameters	LSDA	GGA	Concentration
$a_\circ$(A°)	4.3453	4.453	
$B_\circ$(Gpa)	167	134.8	0.5
B'	4.1	3.9	
$a_\circ$(A°)	4.233	4.3287	
$B_\circ$(Gpa)	286	229	0.75
B'	4.44	4.62	

From the table **4.II.2**, we see that the lattice parameter for x=0.5 with GGA method is greater than the LSDA method by about 0.1077A°. Our calculations for x=0.75 show that the GGA lattice constant is greater than the LSDA of about 0.0947 A°, while the bulk modulus value and its derivative obtained by GGA method is smaller than those obtained by LSDA method. This is the same result for all concentrations and also for the binary compounds. For higher concentrations up to our best knowledge there are no studies for $Al_{0.5}Mn_{0.5}N$ and $Al_{0.25}Mn_{0.75}N$.

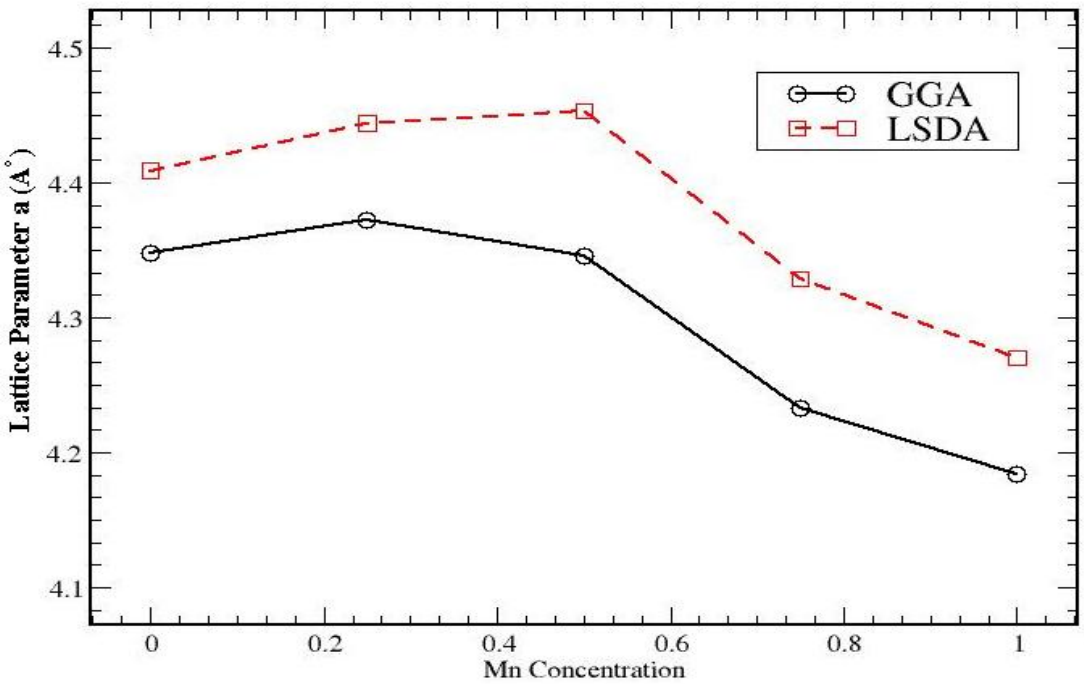

Figure 4.II.4: Equilibrium lattice constants as a function of the Mn concentration for the zincblende $Al_{1-x}Mn_xN$ system in both LSDA and GGA approximations.

Figure 4.II.5 shows us that the lattice parameters of $Al_{1-x}Mn_xN$ alloys depend strongly on the Mn doped atoms concentration. For GGA approximation, the lattice parameter decreases as the Mn concentration increases but deviates at x= 0.25 and x=0.5, the same result with LSDA approximation but deviates only at x= 0.25. The maximum value of the

lattice constant occur at x=0.25, while the minimum at x=1 for the two GGA and LSDA approximations.

4. II.2: Electronic structures

Spin polarized calculations are performed using the concept of spin-up and spin-down electrons separately. Figure 4.II.4, shows the spin polarized band structure of $Al_{0.75}Mn_{0.25}N$ for both spin up and spin down (majority spin and minority spin). New states were found to form within the wide band gap of AlN and convert it from insulator to semiconductor; the majority spin band structure has the same structure as the minority spin except for the region between -2eV to 2.2eV.

For the majority there are bands slightly crossing the Fermi energy with a narrow band gap about 1.218eV and 1.473eV with LSDA and GGA approximation respectively. We define the majority-spin component to be the one that contains the largest number of electrons.

For the minority-spin, the top of the valence band is under the Fermi level and the band gap is much wider 3.491eV and 3.3628eV with LSDA and GGA approaches respectively.

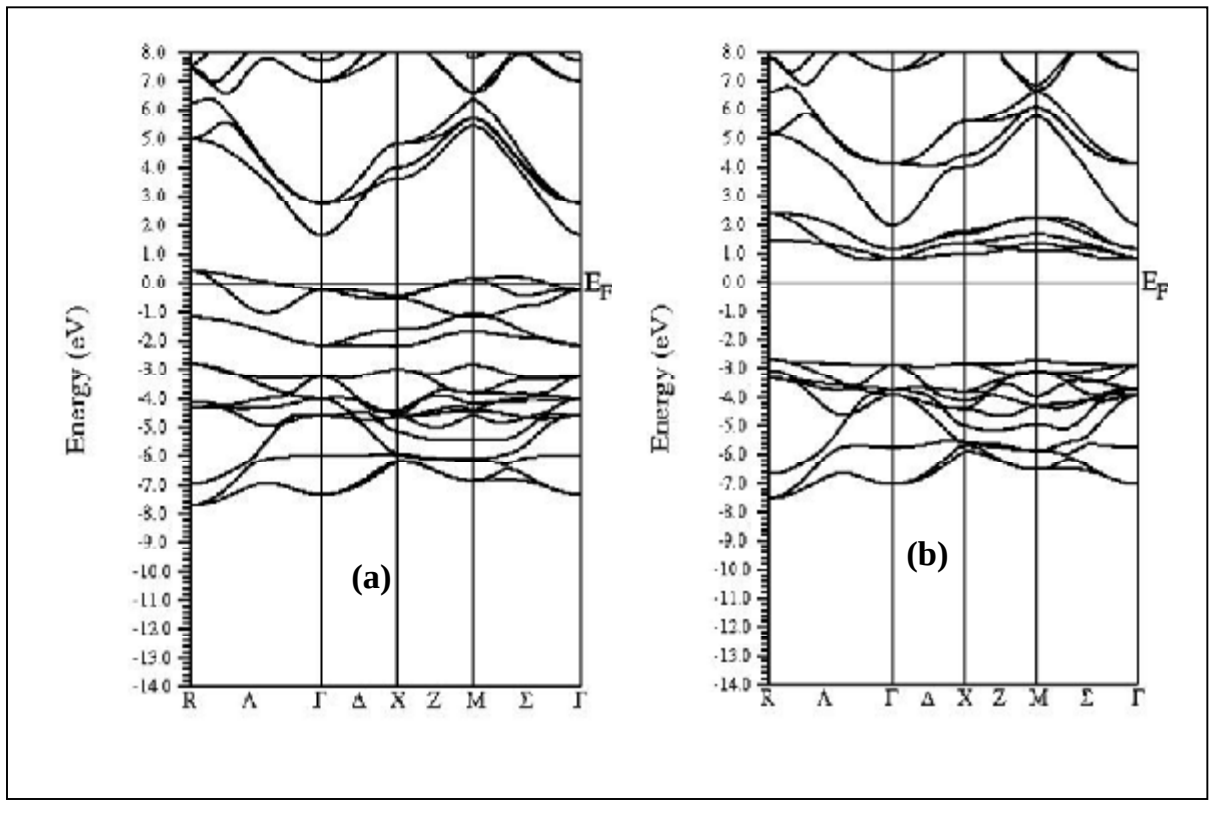

Figure 4.II.5: The spin polarized band structure for $Al_{0.75}Mn_{0.25}N$ in the zincblende structure: a) Majority spin, b) Minority spin.

Figure 4.II.5 and Figure 4.II.6 show us the spin polarized band structure diagram along the high symmetry directions of the Brillouin Zone for $Al_{0.5}Mn_{0.5}N$ and $Al_{0.25}Mn_{0.75}N$; the bands are crossing the Fermi energy for both spin up and spin down (majority spin and minority spin), the Fermi level lies in the band. The system behaves like a ferromagnetic semimetal. Sanyal *et al* [94] study the $Ga_{0.5}Mn_{0.5}N$ in the wurtzite structure, and the calculations show that the system is ferromagnetic metal and it is semi metallic with the other concentrations of Mn (low concentrations).

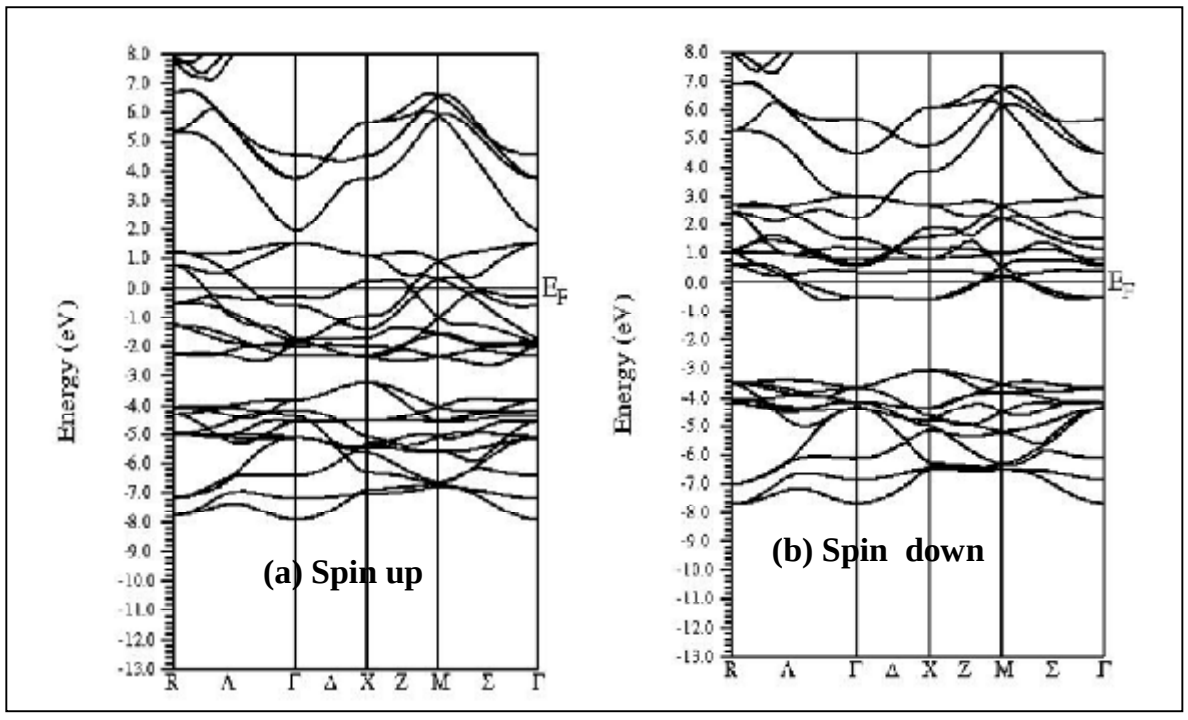

Figure 4.II.6: The spin polarized band structure for $Al_{0.5}Mn_{0.5}N$ in the zincblende structure: a) Majority spin, b) Minority spin.

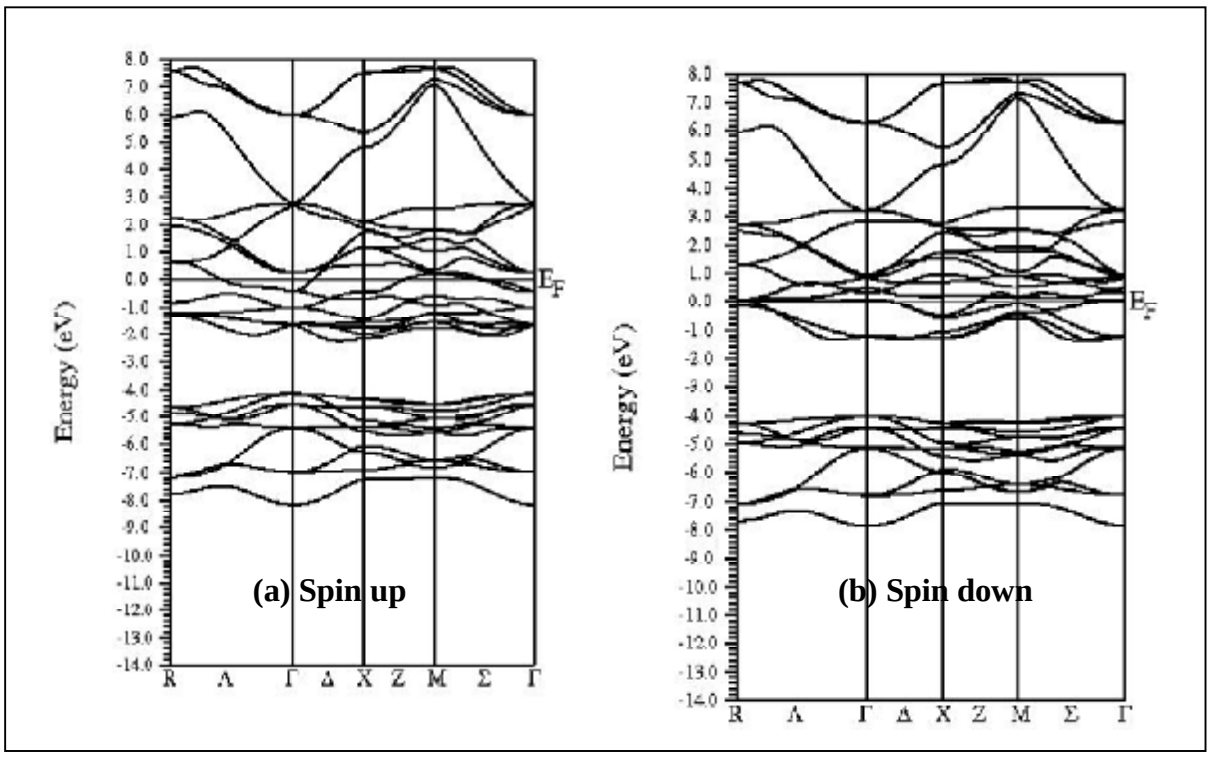

Figure 4.II.7: The spin polarized band structure for $Al_{0.25}Mn_{0.75}N$ in the zincblende structure: a) Majority spin, b) Minority spin.

4.II.3 Density of state (DOS)

Density of state DOS of a system describes the number of states at each energy level that are available to be occupied.

From the total and local partial DOS for $Al_{0.75}Mn_{0.25}N$ Figure 4.II.7 and Figure 4.II.8, we can see that the energy range from -7.8eV to -2.3eV come mainly from Mn-d state and N-p state with a little contribution from Al-p and s states.

For the majority the Mn-d state divided into two parts, the Mn-d doubly degenerate state (d-e_g) has a maximum value between -2.2eV to -0.9eV with a band width about 1.3eV, the Mn-d triply degenerate (d-t_2)band maximum value between -1.3eV to 0.5eV and we can see the Fermi energy running through it. The energy region from -7.7eV to -2.6eV comes mainly from the Mn-d band (triply degenerate (d-t_2) and a small value from doubly degenerate (d-e_g)), and the N-p state with a small contribution from Al-p state.

For the minority, the energy region from 0.48eV to 2.4 eV comes mainly from the Mn-d band (triply degenerate state t_2 and doubly degenerate (e_g) with a small contribution from Al-p and N-p states.

The energy region from -7.75eV to -3eV comes mainly from N-p state and smaller contribution from Mn-d (triply degenerate d-t_2), with a small contribution from Al-p and s states. The top of the valence band for the minority far away below the Fermi energy, while the bottom of the conduction bands are above the Fermi energy.

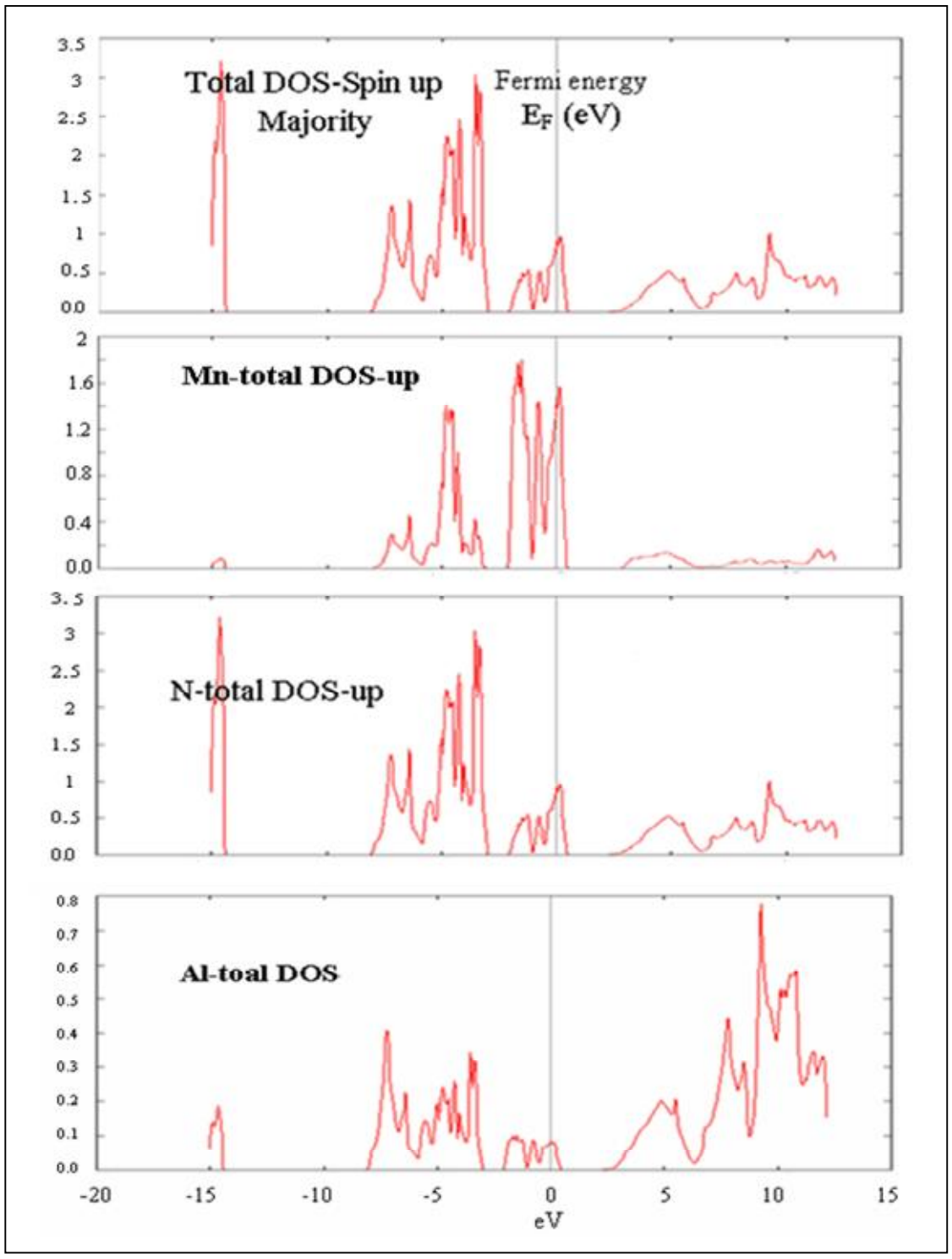

Figure 4.II.8: Total and partial density of states DOS for $Al_{0.75}Mn_{0.25}N$ with spin up (Majority state).

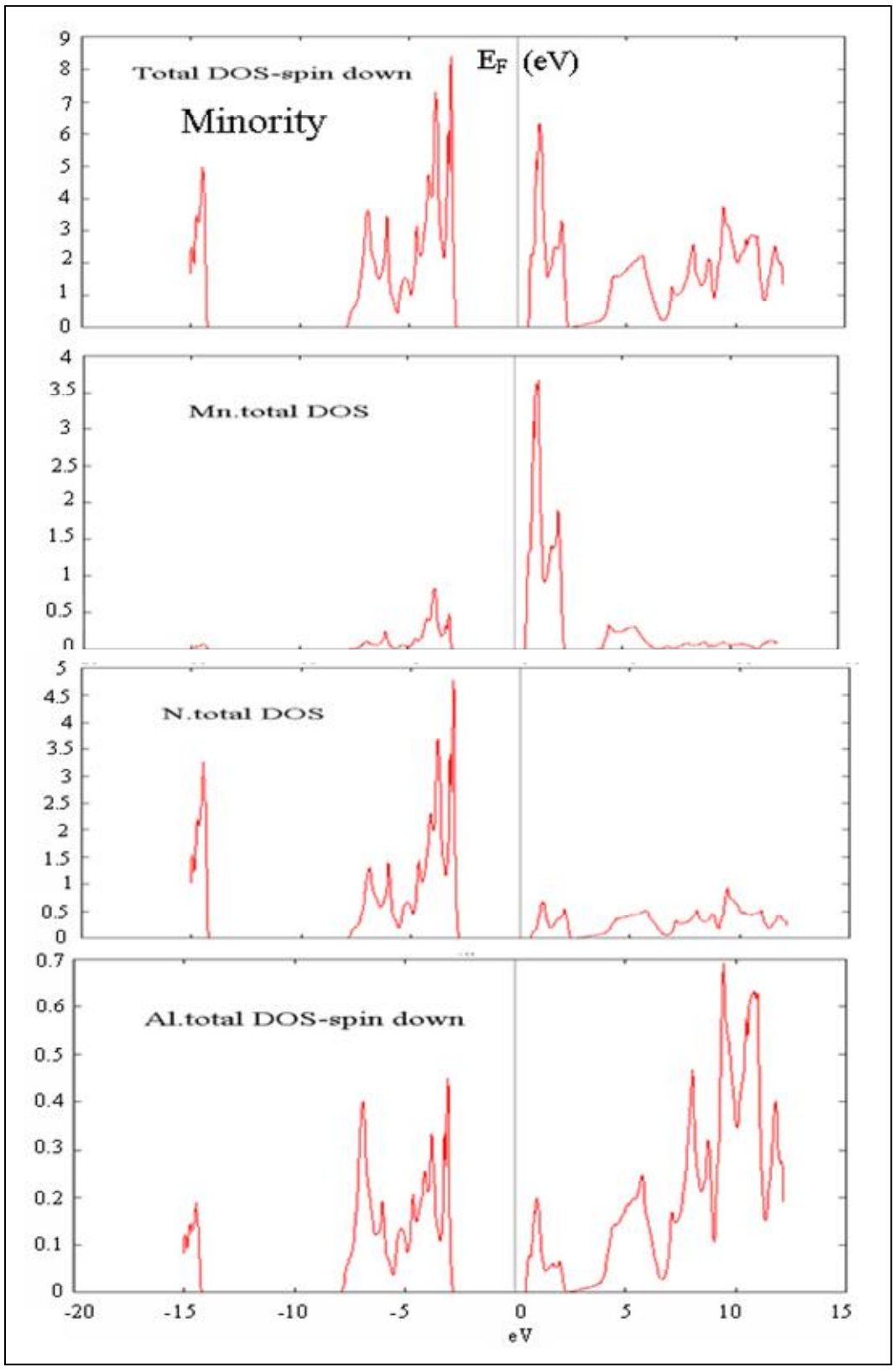

Figure 4.II.9: Total and partial density of states DOS for $Al_{0.75}Mn_{0.25}N$ with spin down (Minority state).

4. II.4: Magnetic properties

The total magnetic moment M^{tot} per unit cell at x=0.25 is $4\mu_\beta$/unit cell with both LSDA and GGA approaches, where μ_β is the Bohr magneton. Kanoun *et al* [46] studied the AlMnN alloy with x=0.25 and calculated the total magnetic moment using FP-LAPW + lo and it was $4\mu_\beta$, so we can see that the present calculation is in good agreement with Kanoun *et al* theoretical calculations. The main value of the total magnetic moment M is strongly localized on the Mn site ($M^{Mn)}$ about $3\mu_\beta$, the remaining value comes from the N and Al atoms, table (4.II.4).The total magnetic moment M^{tot} for $(Al_{0.5}Mn_{0.5}N)$ is about 5.0 μ_β at the equilibrium lattice constant (a_o^{LSDA} =4.3453 A°) using LSDA approach, and it is about 6.839 μ_β at (a_o^{GGA} = 4.453 A°) using GGA approximation.The total magnetic moment calculated with GGA method is greater than LSDA method of about 1.839 μ_β; this is because the equilibrium lattice constant in GGA method is greater than the LSDA method of about 0.1077 A°.

The magnetic moment for $(Al_{0.25}Mn_{0.75}N)$ is about $2\mu_\beta$ at the equilibrium lattice constant (a_o^{LSDA} = 4.233A°) with LSDA method, and it is about 3.125 μ_β at (a_o^{GGA}= 4.3287 A°) with GGA approximation. We can see the difference in the total magnetic moment of about 1.125 μ_β between the two LSDA and GGA approaches. Part of this difference is related to the difference in the equilibrium lattice constant (a_o).

Table (4.II.4) shows that the main value of the total magnetic moment is strongly localized on the Mn site M^{Mn} and is about $3\mu_\beta$, 2.74 μ_β and $1\mu_\beta$ for x=0.25, 0.5 and 0.75 respectively, the remaining values come from the N and Al atoms. We note that the most important role in this system is due to the contribution of the Mn atoms.

Table 4.II.4: Total and local Magnetic moments in $Al_{1-x}Mn_xN$ systems in the zincblende structure using LSDA and GGA approximations.

concentration	**0.0**	**0.25**	**0.5**	**0.75**	**1**
	LSDA Method				
$M^{interstitial}(\mu_\beta)$	**0.00028**	**0.79621**	**0.53957**	**0.31095**	**-0.00621**
$M^{Mn}(\mu_\beta/atom)$	**-0.00002**	**2.92026**	**2.114**	**0.54758**	**------**
$M^{N}(\mu_\beta/atom)$	**-0.00004**	**0.05188**	**0.02463**	**0.0022**	**0.00071**
$M^{Al}(\mu_\beta/atom)$	**--------**	**0.02561**	**0.05343**	**0.03725**	**-0.00045**
$M^{tot.}(\mu_\beta/unit\ cell)$	**0.00022**	**4.00002**	**5.00**	**2.00**	**-0.00599**
concentration	**0.0**	**0.25**	**0.5**	**0.75**	**1**
	GGA Method				
$M^{interstitial}(\mu_\beta)$	**0.10056**	**0.78145**	**1.14652**	**0.28352**	**-0.0118**
$M^{Mn}(\mu_\beta/atom)$	**0.61346**	**3.04205**	**2.7414**	**0.95255**	**--------**
$M^{N}(\mu_\beta/atom)$	**-0.03942**	**0.0302**	**0.03316**	**-0.01023**	**0.00731**
$M^{Al}(\mu_\beta/atom)$	**-------**	**0.02118**	**0.03914**	**0.02466**	**-0.00374**
$M^{tot.}(\mu_\beta/unit\ cell)$	**0.6746**	**4.00**	**6.83935**	**3.1249**	**-0.00827**

The Mn magnetic moment ($\mathbf{M^{Mn}}$) depends on the Mn concentration (depends on the number of Mn atoms per unit cell) Figure 4.II.10 and this difference related to the Mn-Mn spin interaction. The total magnetic moment M^{tot} depends strongly on the Mn concentration and reaches its maximum value with x=0.5. The magnetic moment of Al and N are very small and goes to zero. There is a difference in the total magnetic moment between the LSDA and GGA approximation with x=0.0, 0.5 and 0.75, part of this is related to the difference in the lattice constant value. With the same lattice constant they give us approximately the same value of magnetic moment. The calculated total magnetic moments M^{tot} for MnN

are zero at the equilibrium lattice for both LSDA and GGA approaches as the results by using smaller R_{MT} than we used.

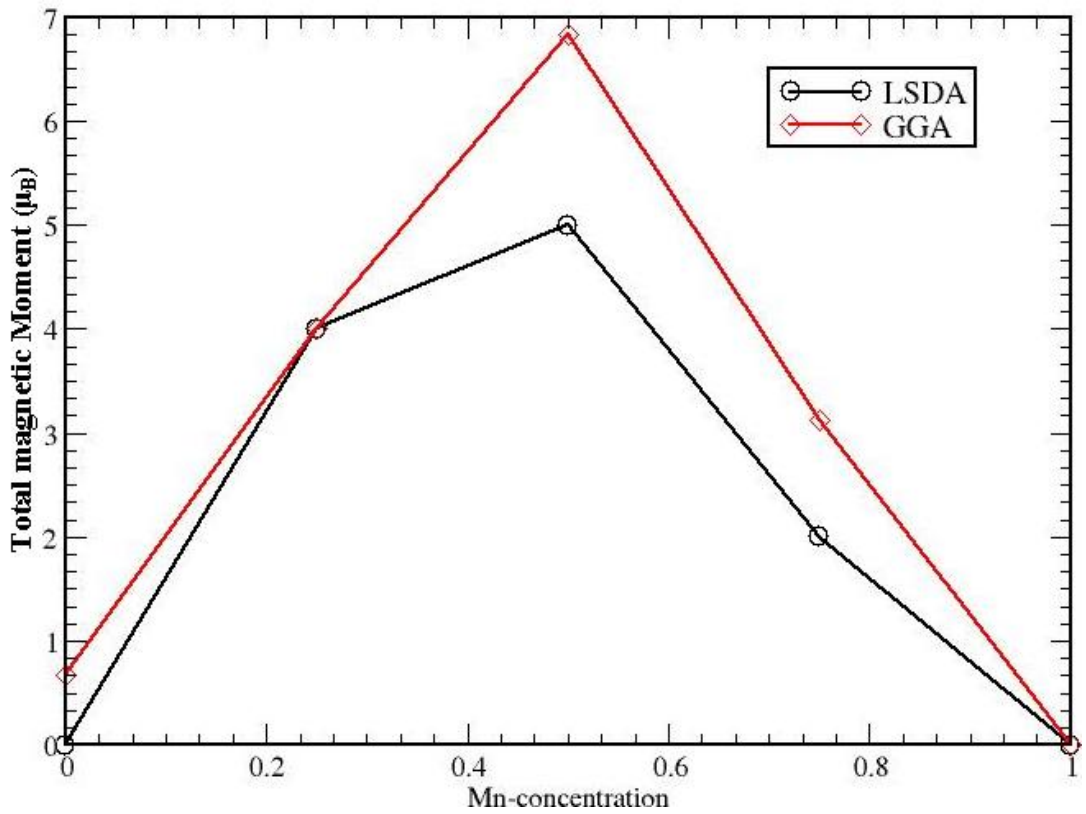

Figure 4.II.10: The total magnetic moment M^{tot} (μ_B/unit cell) of $Al_{1-x}Mn_xN$ as a function of the Mn-concentration in both LSDA and GGA approaches.

Kulatvo *et al* [95], studied the magnetic ordering for GaMnN and GaMnAs with different concentration of Mn using (TB-LMTO) method, the total magnetic moment M was calculated to be 4 μ_B, 8 μ_B, 8 μ_B, and 8μ_B/unit cell for 1.56%, 3.125%, 6.25% and 12.5% concentration of Mn atom respectively for both GaMnN and GaMnAs, from these calculations and present calculations we can say that the total magnetic moment depends strongly on the Mn concentration.

Figure 4.II.11 shows that the magnetization increases as the lattice parameter increases and tends to saturate at the value $8\mu_B$/unit cell in both approaches LSDA and GGA. As it expands, it is still ferromagnetic half-metal. It is noticeable that the LSDA values always tend to be lower than the GGA ones as in the binary MnN compound.

The saturation of the magnetization at the value 8 μ_β may be understood on the basis of a model of charge transfer from Mn-3d to the neighbors N-2p shells [89], this charge transfer is not complete due to the strong interaction originating from the p-d hybridization. The hybridization is reduced as the lattice constant increases and so reaches to a magnetic moment of $8\mu_B$.

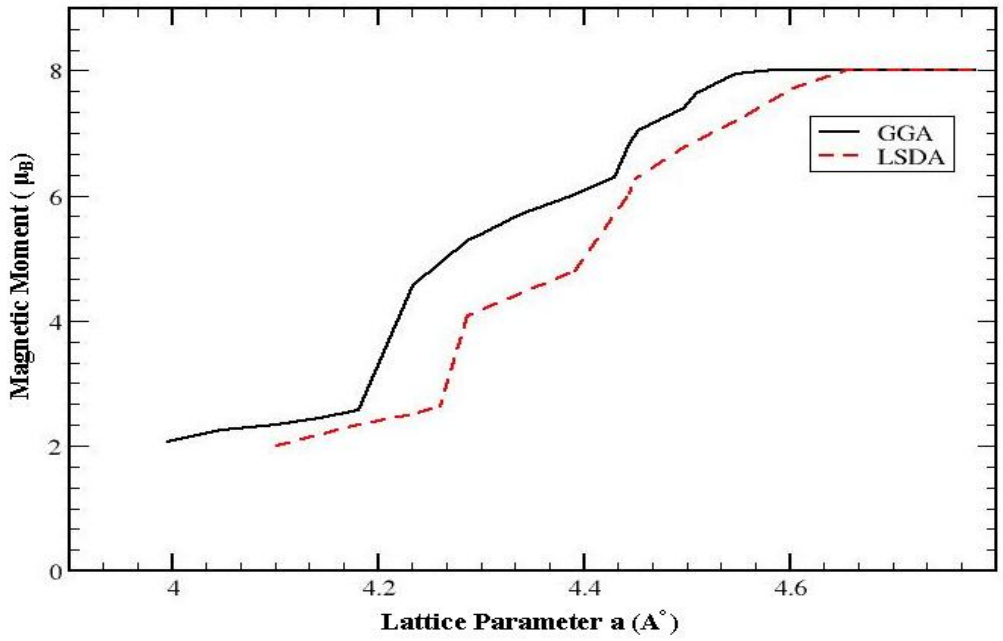

Figure 4.II.11: Magnetization per unit cell for the compounds $Al_{0.5}Mn_{0.5}N$ as a function of the lattice parameter in both LSDA and GGA approaches in zincblende structure.

Chapter five

Summary and Conclusion

The binary compounds (MnN, AlN) and the ternary alloys $Al_{1-x}Mn_xN$ properties are calculated using the self-consistent FP-LAPW method with the LSDA and GGA approximations. We have investigated the equilibrium lattice parameters for different values of Mn concentrations (x = 0.00, 0.25, 0.50, 0.75, 1.00). Our results are in good agreement with the others [46, 26, 20]. The lattice parameters of $Al_{1-x}Mn_xN$ alloys depend strongly on the Mn doped atoms concentration**.**

Upon Mn doping into AlN, new states were found to form within the wide band gap of AlN convert it from insulator to semiconductor or semimetal. With x= 0.25, the majority spin band structure has the same structure as the minority spin except for the region between -2eV to 2.2eV. Fig 4.II.3 shows the spin polarized band structure of $Al_{0.75}Mn_{0.25}N$, for the majority there are bands slightly crossing the Fermi energy level with a narrow band gap of about 1.218eV and 1.473eV with LSDA and GGA approximations respectively.For the minority-spin, the top of the valence band is under the Fermi level and the band gap is much wider 3.491eV and 3.3628eV with LSDA and GGA respectively. With x=0.5 and x=0.75, the valence band crossing the Fermi energy level for both majority-spin and minority-spin as shown in Figures 4.II.6 and 4.II.7.

The total magnetic moment depends strongly on Mn concentration and reaches its maximum value at x=0.5.The main value of the total magnetic moment is strongly localized on the Mn. Also, the magnetization increases as the lattice parameter increases and tends to saturate at the value $8\mu_B$/unit for $Al_{1-x}Mn_xN$ and $4\mu_B$/unit cell for MnN in both LSDA and GGA approaches as shown in Figures 4.I.4 and 4.II.11.

This expansion converts the MnN compound from insulator to semiconductor in which the majority-spin system is metallic and the minority-spin is insulating. We can see that the total magnetic moments for MnN are zero at the equilibrium lattice parameter with LSDA approach but it is about 0.67 μ_β with GGA method. The calculated total magnetic moments M^{tot} for MnN are zero at the equilibrium lattice for both LSDA and GGA approaches as the results by using smaller R_{MT} than we used.

The ferromagnetic (FM) state for the alloys has been found to be more energetically stable than the nonmagnetic state (NM) at x=0.25, $\Delta E_{\circ(NM\text{-}FM)}$ equals 0.13Ry, and x=0.5, $\Delta E_{\circ(NM\text{-}FM)}$ equal 0.12Ry, also from table (5.II.1) the GGA state has been found to be more energetically stable than the LSDA state.

The main results and conclusions of this work are summarized as follows:

1- The calculated structural parameters ($a_\circ$, ***B*** and ***B'***) using FP-LAPW, are found to be in good agreement with the available experimental and theoretical results [46, 82, 83, 85, 88].

2- The equilibrium lattice parameters of $Al_{1-x}Mn_xN$ (x=0.0, 0.25, 0.5, 1.0) alloys are larger for GGA approach than the LSDA approach, while the bulk modulus ***B*** value obtained by GGA approach is smaller than which obtained with LSDA approach.

3- The lattice parameters of $Al_{1-x}Mn_xN$ alloys depend strongly on the Mn doped atoms concentration**.**

4- The energy at equilibrium lattice constant ($E_\circ$) for LSDA method always minimum than with GGA method, this means that these compounds are more stable with GGA approximation.

5- The ferromagnetic (FM) state for the alloys has been found to be more energetically stable than the nonmagnetic state (NM).

6- Upon Mn doping into AlN, new states were found to form within the wide band gap of AlN convert it from insulator to semiconductor or semimetal.

7- The total magnetic moment M^{tot} of $Al_{1-x}Mn_xN$ depends strongly on Mn concentration and reaches its maximum value with x=0.5.

8- The magnetization increases as the lattice parameter increases and tends to saturate at the value $8\mu_B$/unit cell for $Al_{1-x}Mn_xN$ and $4\mu_B$/unit cell for MnN in both LSDA and GGA approaches.

9- The calculated total magnetic moments M^{tot} for MnN are zero at the equilibrium lattice constant for both LSDA and GGA approaches.

10- The calculated total magnetic moments M^{tot} for $Al_{1-x}Mn_xN$ at the equilibrium lattice constant always greater with GGA than LSDA approaches.

Future works

The magnetic moment of all atoms in $Al1_{-x}Mn_xN$ alloys are parallel and the total magnetic moment ranges from 4 μ_B with x=0.25 to about 6.8 μ_B for x=0.5. This unique feature, together with the suggested high Curie temperature, greater than 300 K° [44], makes $Al1_{-x}Mn_xN$ a potential material for spintronics application. So if we can overcome the technological limitations, it may emerge as a significant material for modern spintronics devices.

Moreover these results make a step to future works dealing with superlattice, complex system semiconductors and the problems are not solved up to now.

References

[1] H. Ohno, *Properties of ferromagnetic III-V semiconductors*. **Journal of Magnetism and Magnetic Materials**, **200**(1-3): p. 110-129 (1999).

[2] G. Schmidt and L.W. Mokenkamp, **Journal of Applied Physics**, **89**, 7443 (2001).

[3] R.M. Frazier, G.T. Thaler, B.P. Gila, J. Stapleton, M.E. Overberg, C.R. Abernathy, S.J. Pearton, F. Ren, and J.M. Zavada, **Journal of Electronic Materials**, B **34**, No. 4, (2005).

[4] Y.D. Park, A.T. Hanbicki, S.C. Erwin, C.S. Hellberg, J.M. Sullivan, J.E. Mattson, T.F. Ambrose, A. Wilson, G. Spanos, B.T. Jonker, **Science 295**, 651 (and references therein). (2002).

[5] R.E. Hummel, *Electronic properties of materials*. Third Edition. **New York: Springer**. xvii, 438 p. (2001).

[6] T. Dietl, Ferromagnetic semiconductors. **Semiconductor Science and Technology**, **17**(4): p. 377-392 (2002).

[7] V. Molnar, **Proc. IEEE. 91: p.** 715(2003).

[8] Y. Ohno, D.K. Young, B. Beschoten, F. Matsukura, H. Ohno, D.D. Awschalom, **Nature (London)** 402, 790 (1999).

[9] G. Burkard *et al.*, **Physical. Review**. **B 59**, 2070 (1999).

[10] G. Prinz, , **Journal of Material Science 282**, 1660 (1998).

[11] S. Datta, and B. Das, **Applied Physics Letters**, **56**(7): p. 665-667 (1990).

[12] M. Jain, L. Kronik, and J. R. Chelikowsky. V. V. Godlevsky, **Physical. Review**, **B 64**, 245205 (2001).

[13] S. B. thapa, C. Kirchner, F. Scholz, G.M. Prinz, K. Thonke, R. Sauer, A. Chuvilin, Biskupek, U. Kaiser, D. Hofstetter, **Journal of Crystal Growth** 298, 383-386 (2007).

[14] C.R. Miskys, J.A. Garrido,, C.E. Nebel, M. Hermann, O, Ambacher,

M. Eickhoff, M. Stutzmann, **Applied Physics Letter, 82**, 290 (2003).

[15] Y. Taniyashu, M. Kasu, T. Makimoto, **Applied Physics Letter 84**, 2115 (2004).

[16] O. Madelung, *Physics of III-V Compounds* **(New York: Wiley) p 18** (1964).

[17] W.A. Harrison, *Electronic Structure and the Properties of Solids*, **Dover, New York**, (1989).

[18] A. Garcia and M. L. Cohen, **Physical Review. B 47, 4215** (1993).

[19] M. Mekata, J. Haruna, and H. Takaki, J. Phys. **Soc. Jpn**. **21**, 2267 (1966).

[20**]** R. de paviva, J. L. A. Alves, R. A. Nogueira, J.R. Leite, and L.M.R Scolfaro, Brazilian **Journal of Physics**. **Vol 34**, no 2B, (2004).

[21] K. Suzuki, Kaneko, H. Yoshida, Y. Obi, H. Fujimori, and H.Morita, **Journal of Alloys and Compounds**. **306 (1-2), 66** (2000).

[22] K. Kawaguchi, A. Kuramata, **Jpn. Journal of Physics. L 1400** (2005).

[23] Q. Paduano, D. Weyburne, **Jpn. Journal of Applied Physics. 44 L 150** (2005).

[24] J. Bai, M. Dudley, W.H. Sun, H.M. Wang, M.A, Khan, **Applied Physics Letter 88**, 051903 (2006).

[25] http://nsr.mij.mrs.org./5/6/endnotes.htm#lu-mrssp-482-277

[26**]** R. de paviva, J. L. A. Alves, R. A. Nogueira, J.R. Leite, and L.M.R Scolfaro, **Journal of magnetism and materials**, 288, 384-396, (2005).

[27] S.J. Pearto, C.R. Abernathy, D. P. Norton, A.F. Hebard, Y.D. Park, L.A. Boatner, and J.D. Budai, Mater. **Sci. Eng**., R. **40**, 137 (2003).

[28] E. Matsukura, H. Ohno, and T. Dietl, Handbook of Materials, edited by K. H. J. Buschow (**Elsever Scince, North-Holland, Vol 14**,P.1.

(2002).

[29] H. Munekata, H. Ohno, Von Molnar S, Segmuller A and Chang L L **Physical Review Letter. 63,** 1849 (1989).

[30] H. Ohno, *Making Nonmagnetic Semiconductors Ferromagnetic*, **Science 281, 951** (1998).

[31] H.Ohno, **Journal of Magnetism** and **Magnetic Materials 200**, 110 (2000).

[32] B. Beschoten, P. A. Crowell, I. Malajovich and D. D. Awschalom. **Physical Review Letter 83** 3073 (1999).

[33] M. Jain, L. Kronik, and J. R. Chelikowsky. V. V. Godlevsky, **Physical Review B 64**, 245205 (2001).

[34] S. Sanvito, p. Ordejon and N.A. Hill, **Physical Review B 63** 165206 (2001).

[35] T. Diet, H. Ohno, F. Matsukura, J. Cibert, and D. Ferrand, **Journal of Material Science 287 1019** (2000).

[36] S.G. Yang, A.B. Pakhomov, S.T. Hung, and C.Y. Wong, **Journal of Applied Physics. Letter. B 81**, 2418 (2002).

[37] S.Y. Wu, H.X. Liu, L. Gu, R.K. Singh, L. Budd, M. Schilfgaaarde, M.R. McCartney, D.J. Smith, and N. Newman, **Applied Physics Letter. 82**, 3047 (2003).

[38] V.I. Litvinov and V.K. Dugaev, **Physical Review Letter. 86**, 5593 (2001).

[39] Arkun, Fevzi Edem. *Study of Mn Doped GaN for Spintronic Applications*, **North Carolina State University**. Etd PDF (2006).

[40] R. Frazier, G. Thaler, M. Overbeg,B.GilaC.R. Abernathy and S.J. Pearton **Journal of Physics**. **83**, 1758 (2003).

[41] G.T. Thaler et al., **Applied Physics Lett. 80**, 3964 (2002).

[42] Frazier et al. **Journal of Physics 94** 1592 (2003).

[43] A.L. Chudnovskiy and D. Pfannkuche, **Physical Review** B **65,** 165216 (2002).

[44] M. Van Schilfgaarde and O. N. Mryasov, **Physical Review.** B **63**, 233205 (2001).

[45] R. de Paiva, and R. A. Nogueira **Journal of Applied Physics. vol**. **96**, 6565 (2004).

[46] M.B. Kanoun, S. Goumri-Said, A.E. Merad and J. Cibert, **Journal of Physics. D; Applied Physics. 38**, 1853-1859 (2005).

[47] P. Blaha, K. Schwarz, P. Sorantin, and S.B. Trickey**,** *Full-potential, linearized augmented plane wave programs for crystalline systems***, Compound Physics Communications. 59, 399** (1990).

[48] WIEN2K, *An Augmented-Plane-Wave+Local Orbitals Program for Calculating Crystal Properties*, Karlheinz Schwarz, Techn., Wien, **Austria, ISBN** 3-9501031-1-2, 2001.

[49] H. Hohenberg and W. Kohn, *Inhomogeneous Electron Gas***, Physical Review. 136, B864** (1964).

[50] J.P. Perdew, S. Burke and M.Erzerhof, **Physical Review Letter 77** 3865 (1996).

[51] C.Coulson, **Review Model Physics.** 48, 553 (1960).

[52] Hartree, D. R. (1927) **Proc. Campridge Phil. Soc. 25**, 225, 310.

[53] V. Fock, Z. **Physical Review Letter**. **61**, 126 (1930).

[54] P. Hohenberg and W. Kohn, **Physical Review Letter 136**, B864 (1964).

[55] W. Kohn and L. J. Sham, **Physical Review** 140, Al 133 (1965).

[56] O.Gunnarsson and B.I. lundqvist, **Physical Review. B13**, 4274 (1976)

[57] U. Von Barth and L. Hedin, **Journal of Physics. C 5,** 1629 (1972).

[58] J.C. Slater, **Physical Review Letter. 81** , 358 (1951).

[59] J.C. Slater, *The self-Consistent Field for Molecules and Solids*, (McGraw-Hill, New York, 1974).

[60] S.H. Vosko, L. Wilk and M. Nusair, **Can. Journal of Physics. 58**, 1200 (1980).

[61] D.M. Ceperley and B.J. Alder, **Physical Review Letter**. **45**, 566 (1980).

[62] G.S. Painter, **Physical Review**. B 24, 4264 (1981).

[63] D.C Langreth and M.J. Mehl, **Physical Review Letter**. B **28**, 1809 (1983).

[64] A.D. Becke, **Physical Review Letter**. A 38, 3098 (1988).

[65] J.P Perdew, J.A Chevary, S.H. Vosko, K.A. Jackson, M.R. Pederson, D.J. Singh and C. Filhais, **Physical Review Letter**. B 46, 6671, (1992).

[66] O.K. Andersen, **Physical Review Lett**er. B **12**, 3060 (1975).

[67] E. Sjöstedt, L. Nordström, **D.J. Singh, Solid State Comm**. **114**, 15 (2000).

[68] G.K.H Madsen, P. Plaha, K. Schwarz, E. Sjöstedt, L. Nordström, **Physical Review. B 64**, 195134 (2001).

[69] A.D Becke, **Journal of Chem. Phys. 98**, 5648 (1998).

[70] A.D Boese and N.C Handy, **Journal of Chem. Phys. 114**, 5497 (2001).

[71] J.P. Perdew, K. Burke, and M. Ernzerhof, **Physical Review Letter 77** , 3865 (1996); ibid **78** 1386 (E) (1997).

[72] C., Zener, *Interaction between the D-Shells in the Transition Metals.* **Physical Review**, 1951. **81**(3): p. 440-444.

[73] P.W. ,Anderson**,** *Antiferromagnetism - Theory of Superexchange Interaction.***Physical Review**, **79**(2): p. 350-356 (1950).

[74] J.P. Perdew, Y. Wang, **Physical Review.** B 45 13244(1992) .

[75] H.J. Monkhorst and J.D. pack, **Physical Review.** B **13** 5188, (1976).

[76] F.D Murnaghan, **Proc. Natl. Sci. USA 30**, 244 (1944).

[77] K. Schwarz and P. Baha, **Comput. Mater. Sci. 28**, 259 (2003).

[78] K. Schwarz, **Journal of Solid State Chemistry.** 176, 319 (2003).

[79] G.H.K. Madsen, P. Blaha, K. Schwarz, E. Sjöstedt, L. Nordström, **Physical Review. B64** , 195134-1 (2001).

[80] K.Schwarz, P. Blaha, G.K.H. Madsen, **Comput. Phys.Commun. 147**, 71(2002).

[81] G.H.K. Madsen, B.B. Iversen, P. Blaha, K. Schwarz, **Physical Review. B64**, 195102-1-6 (2001).

[82] R. de pavia, J.L.A.Alves , R.A. Nogueira , J.R. Leite , L.M.R. Scolfaro, **Brazilian Journal of physics, vol. 30**, 568-570, (2003)**.**

[83] Saleh, Farah Ali: *$Ga_{1-x}Mn_xN$ Magnetic Semiconductor: First-Principles Study*. (Unpublished Master's Thesis). **An-Najah National University. Nablus. Palestine,** (2008).

[84] M. Van Schilfgaarde, A. Sher and A.B. Chen, **Journal of Crystal Growth. 178**, 8 (1997).

[85] K. Shimada, T. Sota, and K. Suzuki, **Journal of Applied Physics. 84**, 4951 (1998).

[86] C. Stampfl and C.G. Van de Walle, **Physical Review Letter** B **59**, 5521 (1999).

[87] A. Munoz, K. Kunc, **Physica B 185**, 422 (1993).

[88] A. Trampert, O. Brandt and K. *H. Ploog, in crystal Structure of Group III Nitrides*, edited by J.I. Pankove and T. D. Moustakas, **Semiconductors and semimetals Vol. 50** (Academic, San Diogo 1998).

[89] S. Sanvito and N.A. Hill, **Physical Review. B 62 ,** 15553 (2000).

[90] A.Rubio, J.L Corkill, ML Cohen,E.L. Shirley, and S. G. Louie,

Physical Review. B 48, 11810 (1993).

[91] D. Vogel, P. Krueger, and J. Pollmann, **Physical Review. B55**, 12836 (1997).

[92] S.K. Pugh, D.J.Dugdale, S. Brand and R.A Abram, **Semiconductor Science Technology. 14**, 23 (1999).

[93] Kanoun M B, Goumri-Said S, Merad A E, Merad G, Cibrt J and Aourag H **Semiconductor Science Technology. 19** 1220 (2004).

[94] B. Sanyal, O. Bengone, and S. Mirbt, **Physical Review. B 68**, 205210, (2003).

[95] E. Kulatov, H. Nakayama, H. Mariette, H. Ohta and Yu. A. Uspenskii, **Physical Review.** B **66**, 045203 (2002).

[96] C. Kittel *Introduction to solid state physics, a fifth edition,* published by **John Wiley and sons,** printed in the United States of America QC176.K5 (1976).

Appendix

In the beginning of this present work we built the binary compounds in the ZB structure by building a structure file of two distinguishable atoms Mn and N in the case of MnN or Al and N in the case of AlN.

We must note hear that it's usefully to use the Bohr units in the structure file building; this makes the calculations easer than Angstrom units, also its important to use the lattice type F for the binary MnN and AlN.

The atoms positions in the binary case are:

Position Atom 1: (0.00, 0.00, 0.00) a

Position Atom 2: (0.25, 0.25, 0.25) a

Where:

Atom 1 is Mn in the case of MnN or Al in the case of AlN.

Atom 2 is the N atom.

To build the structure file fore the ternary alloys $Al_{1-x}Mn_xN$ we must use different structure file with eight atoms instead of two atoms, lattice type P and Bohr units.

The atoms positions are:

Position Atom 1: (0.00, 0.00, 0.00) a

Position Atom 2: (0.00, 0.50, 0.50) a

Position Atom 3: (0. 50, 0.00, 0.50) a

Position Atom 4: (0.50, 0.50, 0.00) a

Position Atom 5: (0.25, 0.25, 0.25) a

Position Atom 6: (0.25, 0.75, 0.75) a

Position Atom 7: (0.75, 0.25, 0.75) a

Position Atom 8: (0.75, 0.75, 0.25) a

In the case of x=0.25 there are only one Mn atom in the first position and three Al atoms in the next three positions while the Nitrogen in the last four positions.

In the case of x=0. 5 there are two Mn atoms in the first two positions and two Al atoms in the next two positions while the Nitrogen atoms in the last four positions.

In the case of x=0.75 there are only one Al atom in the first position and three Mn atoms in the next three positions while the Nitrogen atoms in the last four positions.

It is important hear to mention that you haven't to distinguish between these atoms in all concentrations, in other words you haven't to write Mn1, Al1, Al2, Al3 or N1 to N4 except with x=0.5. In the case of x=0.5 you must distinguish Manganese and Aluminum atoms from each other by using Mn1, Mn2, Al1 and Al2 or you will face a problems which not solved else you distinguish them. You haven't to distinguish N atoms in this structure file.

جامعة النجاح الوطنية
كلية الدراسات العليا

دراسة أولية للخصائص الالكترونية والتركيبية والمغناطيسية للمخلوط الثلاثي $Al_{1-x}Mn_xN$ في حالة التركيب زنك بلند

إعداد
رائد توفيق عارف جرادات

إشراف
د. محمد سلامه سالم أبو جعفر
د. عبد الرحمن مصطفى أبو لبده

قدمت هذه الأطروحة استكمالا لمتطلبات درجة الماجستير في الفيزياء بكلية الدراسات العليا في جامعة النجاح الوطنية في نابلس – فلسطين.

2009

دراسة أولية للخصائص الالكترونية والتركيبية والمغناطيسية للمخلوط الثلاثي $Al_{1-x}Mn_xN$ في حالة التركيب زنك بلند

إعداد

رائد توفيق عارف جرادات

إشراف

د. محمد سلامه سالم أبو جعفر
و
د. عبد الرحمن مصطفى أبو لبده

ملخص

نقـدم فـي هـذه الأطروحـة حسـاب الخصـائص المغناطيسـية والالكترونيـة للمخـاليط المغناطيسية $Al_{1-x}Mn_xN$ في حالـة التركيـب البلـوري لكبريتـات الخارصـين ZnS زنـك بلنـد (Zincblende) وذلـك باسـتخدام طريقـة الموجـات المسـتوية المعدلـة الخطيـة لجهـد تـام (FP-LAPW). لقد تـم استخدام تقريـب الكثافـة المغزليـة الموضـعية (LSDA) وتقريـب الميـل الإتجاهي المعمم (GGA) للجهد التبادلي الترابطي.

البرنـامج المستخدم فـي حسـاباتنا هو (WIEN2K-code) وهـو برنـامج خـاص مكتـوب بلغة (Fortran) على نظام التشغيل Linux .

من اهم النتائج التي توصلنا اليها ما يلي:

1- أظهـرت الدراسـة الحاليـة بـأن المركـب AlN ذو طاقـة فجـوة غيـر مباشـرة مقـدارها (3.258eV) و ذو طاقة فجوة مباشرة مقدارها حوالي (6 eV) وهـو مـادة غير موصـلة و لا يمتلك الخصائص المغناطيسية في التركيب البلوري الحالي .

2- تم الحصول على طاقة فجوة متباينـة للمخلـوط $Al_{1-x}Mn_xN$ وتبين بأنها تعتمد على تركيز مادة المنغنيز Mn.

3- لا يوجـد عـزم مغناطيسـي لمركـب نتـرات المغنيسـيوم MnN عنـد حالـة الاتـزان الحجمـي و يمكن له أن يصل إلى حالة المادة المغناطيسية إذا تعرض لظروف تجعله يزداد حجما كرفع درجة حرارته مثلا.

4- العزم المغناطيسي للمخلوط $Al_{1-x}Mn_xN$ يعتمد مقداره على نسبة تركيز ذرات المنغنيز وهو يتراوح بين μ_β 0.0 للتركيز صفر الى حوالي μ_β 6.8 عند التركيز 0.5 لذرات Mn.

5- قيمة العزم المغناطيسي للمخلوط $Al_{1-x}Mn_xN$ وكذلك معامل (ثابت) الشبكة (lattice parameter/constant) اكبر للتقريب GGA مقارنة مع القيم للتقريب LSDA ولكن العكس مع معامل الصلابة bulk modulus فقيمته اكبر مع التقريب LSDA وهذا يتفق مع الدراسات الاخرى.

6- العزم المغناطيسي للمخلوط $Al_{1-x}Mn_xN$ يزداد مقداره مع زيادة حجم المخلوط ليصل الى اعلى قيمه له وهي μ_β 8.